Matematisk-fysiske Meddelelser
udgivet af
Det Kongelige Danske Videnskabernes Selskab
Bind **34,** nr. 8

Mat. Fys. Medd. Dan. Vid. Selsk. **34,** no. 8 (1964)

COULOMB EXCITATION OF LEVELS IN Cu^{63} AND Cu^{65}

BY

B. ELBEK, H. E. GOVE AND B. HERSKIND

København 1964
Kommissionær: Ejnar Munksgaard

CONTENTS

Synopsis

Levels in Cu^{63} at 0.668, 0.961 and 1.327 MeV and in Cu^{65} at 0.770, 1.114 and 1.482 MeV have been studied by the technique of Coulomb excitation, using 36 MeV O^{16} ions. Spin assignments of 1/2, 5/2 and 7/2, respectively, for the two sets of levels were made, based on angular correlations of the cross-over gamma rays to the ground state measured in coincidence with O^{16} ions scattered into a counter near 180°. Relative $B(E2)$ for the levels in Cu^{63} as given above were found to be 1.00, 1.01 ± 0.03 and 1.10 ± 0.03, while that for the 1.862 MeV level was less than 0.2 (assuming $J = 3/2$). In Cu^{65} the values were 1.00, 1.11 ± 0.04 and 0.97 ± 0.03, while that for the 1.623 MeV level was less than 0.2 (again assuming $J = 3/2$). The absolute values of $B(E2)$ for decay of the 0.845 Mev level in Fe^{56}, the 0.668 Mev level in Cu^{63} and the 0.770 Mev level in Cu^{65} were measured to be 0.019, 0.021 and 0.016 (in units of $e^2 \times 10^{-48}$ cm^4), respectively. The 1.327 Mev level in Cu^{63} branches to the 0.668 Mev level with a 9 % probability and the 1.482 Mev level in Cu^{65} branches to that at 0.770 Mev 24 % of the time. $E2$–$M1$ amplitude ratios for the transition between the 5/2-level and the ground state in both nuclei were measured to be −0.2. Estimates were made of various second-order Coulomb excitation effects which can change the relative $B(E2)$. The experimental results are considered in relation to various current core excitation models.

PRINTED IN DENMARK
BIANCO LUNOS BOGTRYKKERI A/S

1. Introduction

In regions of the periodic table where the low energy spectra of even-even nuclei can be approximately described as quadrupole vibrations one may attempt to analyze the spectra of odd-mass nuclei in terms of such vibrations coupled to the motion of the last odd particle. The understanding of such a system is, of course, a central problem in nuclear physics but, in spite of this, relatively little progress has been made in the experimental and theoretical investigation of the coupled system.

This paper describes some measurements on the low lying levels in the two isotopes of copper, Cu^{63} and Cu^{65}. In these nuclei there are several indications that the low levels are due to the coupling of the odd proton ($p_{3/2}$) in the ground state to the $2+$ excited state of the even-even core. The phenomena associated with this coupling might here be especially well displayed as the odd proton is the only particle outside the closed $f_{7/2}$ shell.

If a coupling of the type discussed here is very weak it would give rise to a degenerate multiplet in the energy spectrum of the nucleus. The spins of the states in this multiplet would be those possible from the vector coupling of the particle angular momentum j to the angular momentum 2 of the quadrupole vibration (Fig. 1). The downwards reduced transition probabilities would all be equal as they correspond to a one-phonon transition which leaves the odd particle unaffected. The states will therefore have the large reduced transition probabilities characteristic of the vibrational excitation in the even-even nucleus. Other excited states correspond to a shift of the odd particle from one orbit to another, but these transitions proceed by approximately single-particle strength.

However, this simple picture can hardly be expected to reproduce the properties of real nuclei. A significant coupling is expected due to the fact that, when the nucleus vibrates, there are corresponding fluctuations in the shape of the field in which the particle moves. To leading order, the coupling is proportional to the amplitude of the nuclear vibration. An estimate of the strength of the coupling together with the empirically determined vibra-

tional parameters show that the conditions for the validity of the weak coupling picture are far from being fulfilled.

It is then necessary to carry the calculations to higher orders, thereby including higher phonons. Such calculations are in general very complicated but, for the special case $j = 3/2$, BAYMAN and SILVERBERG[1] have been able to solve the problem exactly. Their calculation shows that the 1/2, 5/2 and

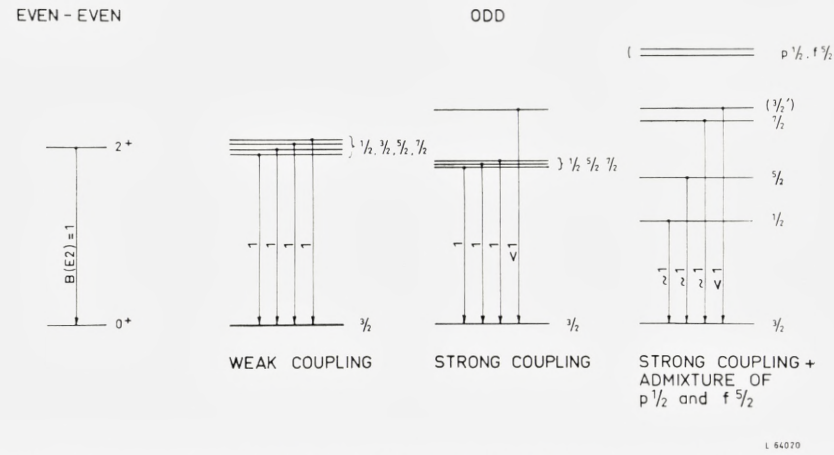

Fig. 1. Schematic representation of the low-lying energy levels in the copper isotopes for different types of particle-vibration coupling.

7/2 states stay degenerate independent of the coupling strength, whereas the 3/2 state increases in energy as the coupling strength increases (Fig. 1). The $B(E2)$ value of the degenerate states are only slightly affected by the coupling in contrast to the $B(E2)$ value of the 3/2 state which is markedly reduced.

Calculations such as those mentioned above still represent a simplification in two respects: a) They assume that the nuclear vibration resembles that of a harmonic oscillator. From the experimental information available[2, 3] it is clear that, although higher phonon states indeed may be found, major deviations from the simple harmonic picture exist. It is at present impossible to take these deviations into account. b) It must be expected that the presence of other single-particle states also gives rise to changes in the orbit of the last odd particle.

In the case of the copper isotopes the most important single-particle states are the $p_{1/2}$ and $f_{5/2}$. This type of coupling has been studied by BOUTEN

and VAN LEUVEN[4]. Their calculation shows that the 1/2 and 5/2 excited states of the multiplet get a considerable contribution from the corresponding single-particle states if the experimentally observed level positions are to be reproduced. The 7/2 level, however, is an almost pure configuration of excited core and $p_{3/2}$ particle.

Another indication of strong admixtures from other single-particle states comes from the recent experiments on the $Ni^{62}(He^3,d)Cu^{63}$ reaction by BLAIR and ARMSTRONG[5]. From these measurements it appears that the 1/2 state in Cu^{63} carries most of the single-particle $p_{1/2}$-strength. Similarly, the 5/2 state gets a significant contribution from the $f_{5/2}$ single-particle level.

These results are qualitatively but not quantitatively in agreement with the wave functions calculated by BOUTEN and VAN LEUVEN. It is of some interest to understand how these data can be brought into agreement with the other features of the Cu-spectra which so strongly support the interpretation in terms of a particle coupled to a vibration.

In the discussions of spectra of the type considered here reference is often made to a "center-of-gravity" theorem[6, 7]. This theorem can be derived in two simple limiting cases: a) If the ground state and the excited state of the core can both be described in terms of the same $(j)^n$ configuration, and if this core interacts with the particle in a definite orbit $j' \neq j$ which is not identical to those of the core particles. b) If the coupling between the core and the odd particle is linear in the vibration amplitude (for harmonic vibrations), and if the single particle is confined to a definite orbit the energy shifts are of second order in the coupling and leave the center-of-mass unchanged.

One hardly expects any of these conditions to be very well realized especially since one must in general expect significant couplings to other single-particle states. Also the experimental evidence, which is most complete for nuclei with spin 1/2, shows that usually the center-of-mass shift is comparable with the splitting between the two first excited states.

Coulomb excitation immediately suggests itself as a method of testing the ideas outlined in the introduction, and in the present paper an account is given of some measurements of the Coulomb excitation of Cu^{63} and Cu^{65}, using a beam of O^{16} ions from the tandem accelerator at the Institute for Theoretical Physics, Copenhagen. The energy levels of both nuclei have been previously measured in some detail[8] and the first two excited states had been studied by Coulomb excitation[9]. Information about the spins of the first two levels had been inferred from β-ray measurements[10], but without great certainty. It was therefore decided to carry out Coulomb

excitation angular correlation measurements as well in order to make unambiguous spin assignments. The use of O^{16} ions as the bombarding particle permits higher excited states to be measured with greater ease than when lighter bombarding particles are employed. In the case of 35 Mev O^{16} ions incident on Cu^{65}, the parameter $\xi^{(11)}$ on which the cross section is sensitively dependent has a value of 0.69 for a level at an excitation energy of 1.623 Mev and, of course, smaller values for lower excited states. This means that the cross section for Coulomb excitation of a level at this energy is sufficiently great to be detected rather readily, provided, of course, that the reduced quadrupole matrix element is of the same order of magnitude as that for the lower levels[9].

2. Experimental Method

A schematic diagram of the apparatus used in these experiments is shown in Fig. 2. The beam of O^{16} ions from the tandem accelerator, focussed by two quadrupole lenses, 2 meters and 14 meters, respectively, from the exit of the 90° analyzing magnet is incident on the target chamber shown in Fig. 2, located 19 meters from the analyzing magnet. Two tantalum apertures are employed, the second of which insures that no beam strikes the particle counters. Thick targets were used and all the beam collected by the insulated target was measured. For most of the experiments 36 Mev O^{16} ions in the charge five state were used and the beam currents were approximately 0.1 μa or less.

The geometry employed for the particle detectors is shown in the inset of Fig. 2. Two gold-surface barrier devices[12], 12 mm × 6 mm in area, separated by 6 mm were connected in parallel to the input of a charge sensitive pre-amplifier[13]. From the output of this pre-amplifier the signal went to a slow amplifier and to fast amplifiers[14]. The latter fed one input of a time-to-pulse height converter which provided a coincidence resolving time of about 20 nano-seconds, while the former after further amplification and clipping passed through a single-channel analyzer, a slow coincidence circuit and gate to a 512 channel analyzer. A combined fast-slow pre-amplifier on the gamma spectrometer provided signals to the other input of the time-to-pulse height converter after amplification in a fast amplifier[14] and to a slow amplifier and single-channel analyzer which, in turn, was connected to the slow coincidence and gate. After amplification, the coincidence pulse from the time-to-pulse height converter passed a single-channel analyzer and then the slow coincidence and gate. This latter unit

was arranged so that the multi-channel analyzer could examine the direct particle, gamma or time spectrum as well as anyone of the three coincident spectra with discriminator gates set on particular portions of the direct spectra from the other two.

The gamma-ray detector, as shown in Fig. 2, was a 7.6 cm diameter by 7.6 cm long NaI crystal optically coupled to an EMI 9531A photomulti-

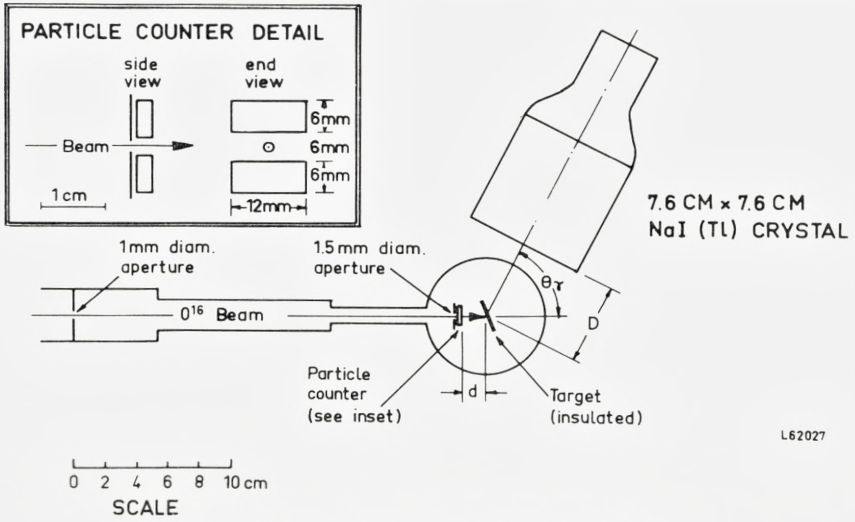

Fig. 2. Scheme of angular correlation apparatus.

plier. This counter could be rotated in angle about the target center and at each angle the gamma ray spectrum was recorded, in coincidence with a gate set on the particle spectrum and on the time spectrum. Since thick targets were employed, the particle spectrum was relatively flat up to pulse heights corresponding to the O^{16} ions back scattered from the target surface, and then fell off rapidly. The gate on this spectrum was usually adjusted to include the upper third of the pulses.

Measurements were made with two different combinations of particle-counter and gamma-counter distances to the target. In the first series of runs these distances were 9 mm and 46 mm, respectively, and in the second 15 mm and 58 mm, respectively. The second set was chosen because the first gave too large an attenuation of the coefficient of the fourth-order Legendre polynomial in the angular distributions. The coincident angular correlations were measured with the gamma counter set at every 10° from

0° to 90°. It was found that, in the first series of runs, because of gain drifts in the particle counter, it was not possible to measure angular correlations reliably without normalizing to the intensity of the gamma-ray line resulting from de-excitation of the first excited states of Cu^{63} or Cu^{65} which have $J = 1/2$ and, hence, give rise to spherically symmetric angular correlations. In the second series of experiments this problem was overcome by using

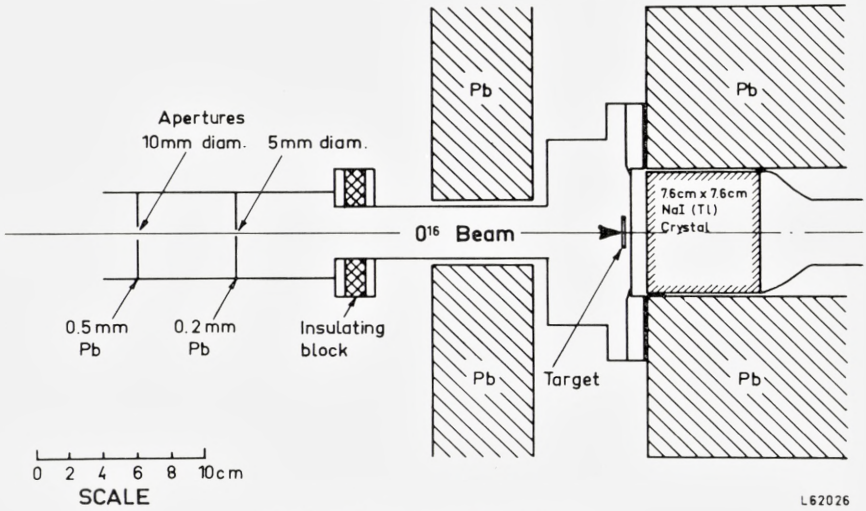

Fig. 3. Scheme of yield apparatus.

a second 7.6 × 7.6 cm NaI(Tl) crystal at a fixed angle, parallelling its output to that of the moving crystal into the fast coincidence part of the circuit and recording its gamma spectrum in a 256 channel analyzer in coincidence with the same gate on the particle spectrum. Any shift in the gain of the particle counters caused equal fractional changes in both coincident gamma spectra.

In addition to the coincident angular correlation measurements described above two other types of measurements were made. The direct yield curves of the gamma rays from the thick target Coulomb excitation of levels in Cu^{63} and Cu^{65} were measured with O^{16} ions from 24 to 40 Mev by means of the experimental arrangement shown in Fig. 3. In this experiment, the 7.6 × 7.6 cm crystal was placed at 0° to the beam and about 13 mm from the target. The Faraday-cup nature of the target chamber ensured that an accurate measurement of the beam current could be made.

Finally, some gamma-gamma coincidence measurements were made, as will be described subsequently. For these measurements a 7.6×7.6 cm NaI crystal and pre-amplifier were substituted for the particle counter in the circuit.

The targets employed were thick targets of both natural copper and the separated isotope of Cu^{65}[15]. The latter was prepared[16] by an electroplating technique. The Cu^{65} oxide powder was converted into another form of the oxide which dissolved readily in H_2SO_4. The electroplating solution comprised $Cu^{65}SO_4$, sodium oxalate, triethanolamine, and water. The copper was electroplated on gold, using a platinum anode. Five hours of electroplating produced a target about 0.5 cm^2 with an areal density of 13.5 mg/cm^2. About 35 % of the isotope was recovered.

In some of the preliminary experiments, thin (about 1 mg/cm^2) self-supporting foils of the separated isotopes of both Cu^{63} and Cu^{65} were used.

3. Coulomb Excitation Theory

a) Angular Distribution

Because of the particle-counter geometry employed in this experiment (see Fig. 2), particularly its large solid angle and lack of cylindrical symmetry about the beam axis, it is not possible to use the simplified expressions of Litherland and Ferguson[17] for a particle counter at 0° or 180°. It is, however, of some interest to compare their expression with that for pure Coulomb excitation obtained by Alder et al.[11], and such a comparison is made in Appendix I. Expressions for the actual theoretical angular distributions for the particle-detector geometries employed in the present experiment are also derived in Appendix I. To compare these expressions with experiment, however, it is necessary to know the values for Q_2 and Q_4, the attenuation constants which take account of the finite geometry of the gamma detector. If the complete area under the measured spectrum of a monoenergetic gamma ray is calculated at each angle, then the attenuation coefficients of Rutledge[18] can be used directly, but in the case of a complex spectrum comprising several gamma rays it is much more convenient and accurate to measure the area under the total absorption peak alone. Since total absorption of the gamma rays is more likely to occur near the center of the crystal rather than near the edges, one would expect the actual attenuation factor to be larger (ɔ: less attenuation) than the computed ones and, further, one would expect the percentage difference to be greater for

Q_4 than for Q_2. It is therefore useful to measure these coefficients, and this was accomplished in the case of the second geometry employed (particle counter 15 mm from the target and gamma counter 58 mm away) by measuring the coincidence angular correlation of 845 kev gamma rays resulting from the Coulomb excitation of the first excited state in Fe^{56} by 33 Mev O^{16} ions. Since the ground and first excited state of Fe^{56} have $J = 0+$ and $2+$, respectively, both the excitation and decay are pure $E2$. Further-

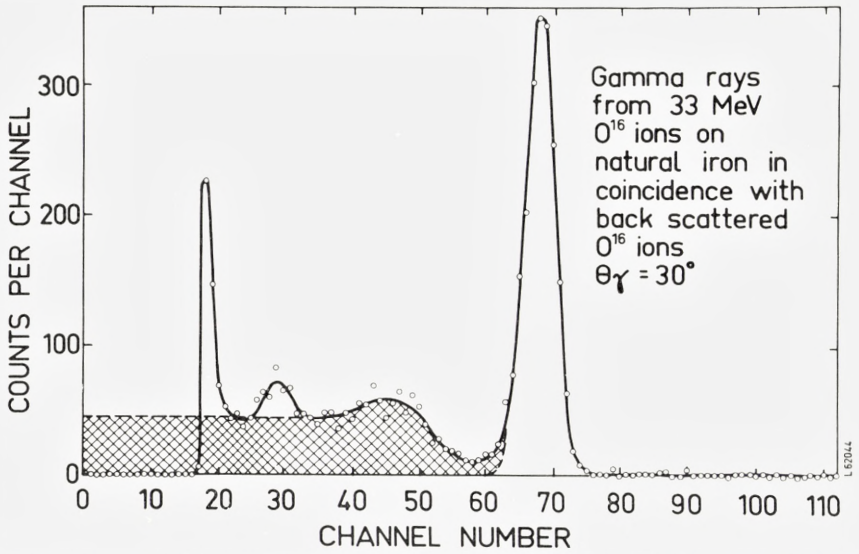

Fig. 4. Spectrum of 845 kev gamma rays from 33 Mev O^{16} ions on a thick natural iron target measured at 90° in coincidence with back scattered O^{16} ions. The counter distances were $d = 15$ mm and $D = 58$ mm, respectively (see Fig. 2). The two ways of measuring the area are indicated.

more, theory predicts both a large coefficient of P_2 and of P_4 in the coincidence correlation. The coincident gamma-ray spectrum is shown in Fig. 4; indicated on this figure are the two methods of measuring the area, in the first case all the pulses in the spectrum were counted and in the second only those in the total absorption peak. In this measurement a monitor counter measured the coincident counting rate at a fixed angle; the resulting angular correlations normalized by the monitor counter are shown in Fig. 5. The solid curves are least square fits of the data to a Legendre polynomial expansion of the form given by equation (20) in Appendix I. For a 7.6 cm × 7.6 cm NaI(Tl) counter at 58 mm from the target the tables of RUTLEDGE[18] give values of the attenuation coefficients Q_2 and Q_4 of 0.84 and 0.53, re-

spectively. The table of ALDER et al.[11] gives $A_2^{(2)} = 0.3571$ and $A_4^{(2)} = 1.143$ for a $0-2-0$ gamma-gamma correlation. Substituting these values, equation (20) of Appendix I results in the coefficients listed in the column

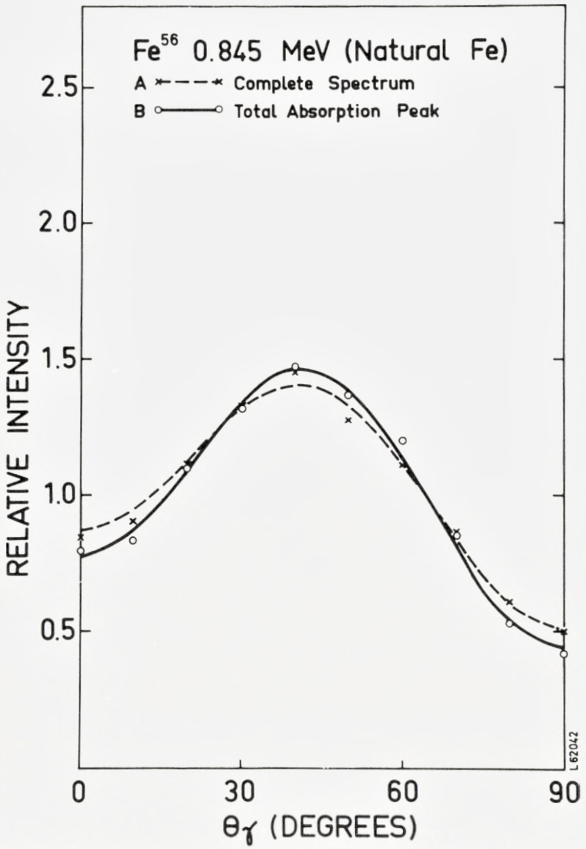

Fig. 5. Angular correlations of 845 kev gamma rays from 33 Mev O^{16} ions on a thick natural iron target measured in coincidence with back scattered O^{16} ions. The counter distances were $d = 15$ mm and $D = 58$ mm, respectively (see Fig. 2). Correlation A involved measuring all the pulses in the spectrum, while for B only the area under the total absorption peak was taken.

headed "theoretical values" in Table I. Agreement with the experimental coefficients derived from the total spectrum is quite good in consideration of the uncertainty of the total number of counts in the gamma spectrum. This comparison confirms that the method of averaging over the particle-counter area is valid.

TABLE I.

Coincidence correlations for $Fe^{56}(O^{16}, O^{16}, \gamma)' E_\gamma = 0.845$ Mev, using 33 Mev O^{16} ions and counter spacings $d = 15$ mm $D = 58$ mm.

	Theoretical values	Experimental values using complete spectrum	Experimental values using total absorption peak only
a_2/a_0	0.490	$0.506 \pm .039$	$0.524 \pm .020$
a_4/a_0	-0.638	$-0.638 \pm .047$	$-0.768 \pm .024$

$$W(\theta) = 1 + a_2/a_0 P_2(\cos\theta_\gamma) + a_4/a_0 P_4(\cos\theta_\gamma)$$

In this comparison between experiment and theory, of course, it has been assumed that first-order Coulomb excitation was dominant. Second-order effects due to re-orientation of the nucleus in its excited 2+ state before emission of the gamma ray can be appreciable under certain conditions. Such effects are discussed in Appendix II, but their chief influence is on the cross section measured at 180° and is negligible as far as the coincident angular correlations are concerned.

One can now compare the theoretical expression of equation (20), Appendix I, with the experimental coefficients listed in the fourth column of Table I, obtained when only the area under the total absorption peak is measured allowing Q_2 and Q_4 to be unknown parameters. This results in values of Q_2 and Q_4 equal to 0.91 ± 0.05 and 0.64 ± 0.02, respectively. Comparing these with the Rutledge values one notes that, although Q_2 is only increased by about 9 %, Q_4 is increased by 20 %. This effect has also been considered recently by ECCLESHALL et al.[19]. Our results for the attenuation factors are collected in Table II. The values of Q_2 and Q_4, actually employed to fit the angular distributions in copper measured in the same geometry, were 0.91 and 0.66, respectively.

TABLE II.

Attenuation factors for the 0.845 Mev γ-ray in Fe^{56}.

	Theoretical values	Experimental values for complete spectrum	Experimental values for total absorption peak only
Q_2	0.836	0.860	0.908
Q_4	0.530	0.532	0.640

Prior to this, however, preliminary measurements of the copper angular distributions were made with the particle- and gamma-counter distances 9 mm and 46 mm, respectively. These measurements, as will be discussed later, allowed spin assignments but not multipole mixing ratios to be measured.

b) Thick Target Yields

The use of thick targets for an absolute determination of $B(E2)$ necessitates an integration of the theoretical cross section for $E2$-Coulomb excitation over the range of the projectile. This means that the following integration has to be performed:

$$Y(E) = B(E2) \times c_{E2} \int_0^{R(E)} E(x) f_{E2}(\xi(E(x)))dx. \tag{2}$$

Here, $Y(E)$ is the thick target yield per incident particle at the energy E, $R(E)$ is the range of the projectile, and c_{E2} a numerical constant. The function $f(\xi)$ is tabulated in ALDER et al.[11].

If one introduces the differential energy loss $-dE/dx$, one can in the usual way change (2) into an integral, $F_{E2}(E)$, over energy

$$F_{E2}(E) = \int_0^E \frac{E f_{E2}(\xi(E))}{dE/dx} dE. \tag{3}$$

In principle, this integral must be evaluated for each combination of projectile, target and excitation energy. However, for practical purposes, certain simplifications are possible[20].

It is first noted that ξ can be split into two factors, one containing the bombarding energy only, whereas the other depends on the particular experimental situation. If the energies are in Mev,

$$\xi = \Lambda \frac{1}{E^{3/2}}; \quad \Lambda = \frac{Z_1 Z_2 A_1^{1/2} \Delta E'}{12.65}, \tag{4}$$

where indices 1 and 2 refer to projectile and target, respectively. The expression $\Delta E' = E(1 + A_1/A_2)$ is a reduced excitation energy.

Secondly, the differential energy loss for any element to a good approximation can be related to the energy loss in a standard material. If

gold ($Z = 79$) is chosen as standard material, the differential energy loss in an element with atomic number Z is[20]

$$\left(\frac{dE}{dx}\right)_Z = \left(\frac{dE}{dx}\right)_{Au} \frac{116}{Z+37}. \tag{5}$$

The values of $-dE/dx$ for gold used in the evaluation of (3) are given in Table III.

By use of the simplifications outlined above one can evaluate the integral (3) for a few values of A covering the range of practical interest ($0 < A < 300$) and then interpolate for other values of A. In this way,

TABLE III.

dE/dx in units of Mev/cm^2/mg for O^{16} ions in gold

E(Mev)	$-dE/dx$
0	2.08
10	2.20
20	2.38
30	2.44
40	2.30
50	2.15

universal integrals are obtained, which for a given projectile easily permits determination of the thick target yield for any excitation energy, and by means of (4) and (5) for any target material.

The $F_{E2}(E)$ for oxygen ions is given in Fig. 6. Expressed by means of the $F_{E2}(E)$ the thick target yield per incident ion is

$$Y(E) = 2.88\times10^{-3}(1 + A_1/A_2)^{-2} \frac{A_1}{A_2 Z_2^2} \frac{Z_2 + 37}{116} F_{E2} \times B(E2). \tag{6}$$

The measured thick target yields of gamma rays per incident O^{16} ion can then be compared to the values obtained from (6) and the values of $B(E2)$ deduced. In practice, as will be described below, the relative $B(E2)$'s for the various levels excited in Cu^{63} and Cu^{65} were calculated from the angular correlations measured in coincidence with back scattered O^{16} ions in the first geometry. Absolute cross sections and from these absolute $B(E2)$'s for excitation of the 0.668 Mev level in Cu^{63} and the 0.845 Mev level in Fe^{56} were measured in the apparatus shown in Fig. 3.

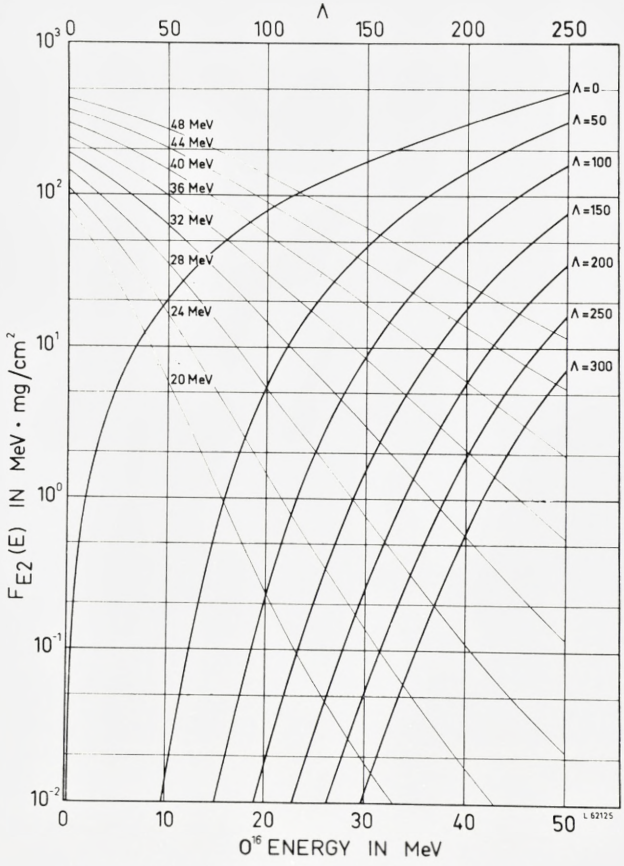

Fig. 6. Thick target yields for O^{16} ions on gold.

4. Experimental Results

a) Relative and Absolute Yields

As mentioned previously, two geometrical arrangements were used in measuring gamma-ray correlations from copper in coincidence with back scattered O^{16} ions. In the preliminary experiments the distance between particle counter and target and gamma-ray counter and target were 9 mm and 46 mm, respectively (distances d and D on Fig. 2). No coincidence monitor counter was available for these preliminary experiments.

Despite the rather poor geometry and the lack of a monitor it was decided to measure the coincidence angular distributions principally to obtain re-

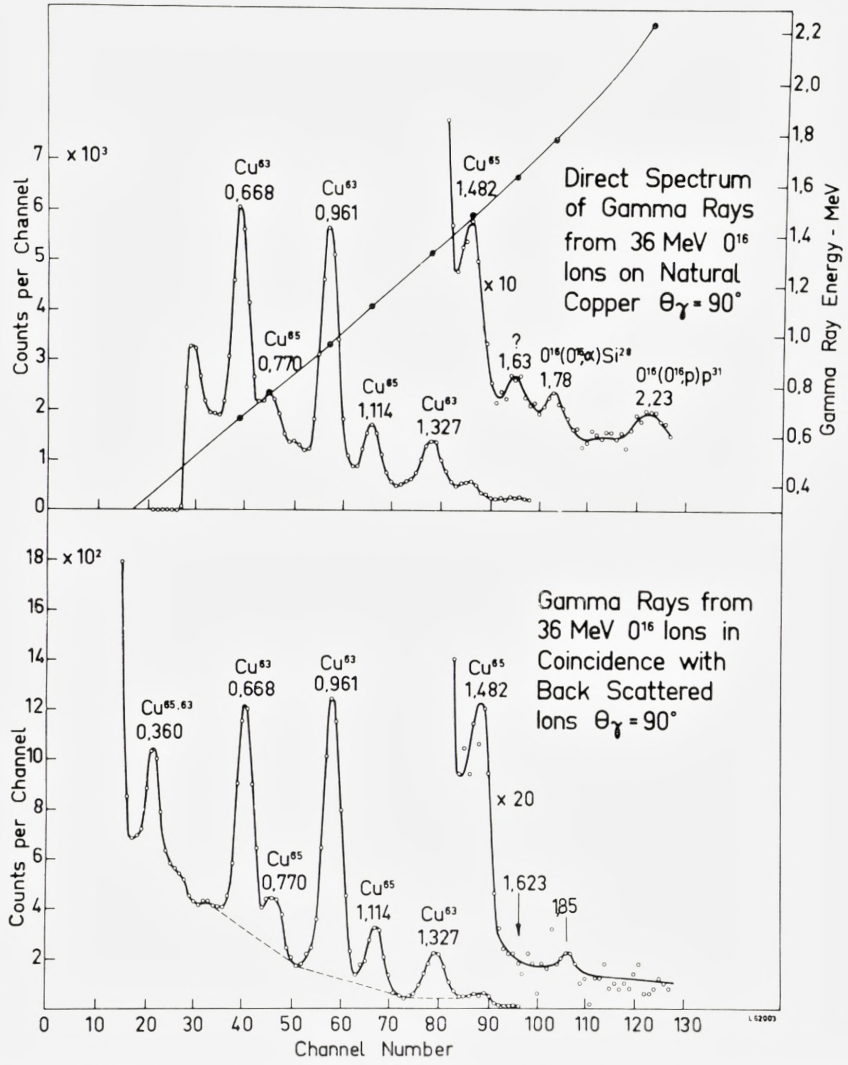

Fig. 7. Direct gamma-ray spectrum (top half of figure) and the gamma ray spectrum in coincidence with back scattered ions (bottom half of figure) are shown for 36 Mev O^{16} ions incident on a thick natural copper target.

lative intensities of the various gamma rays and, in analyzing these distributions, to normalize to the intensity of the gamma ray arising from the de-excitation of the first excited state (at 668 kev in Cu^{63} when a natural copper target was used and at 770 kev in Cu^{65} when a separated Cu^{65} target was

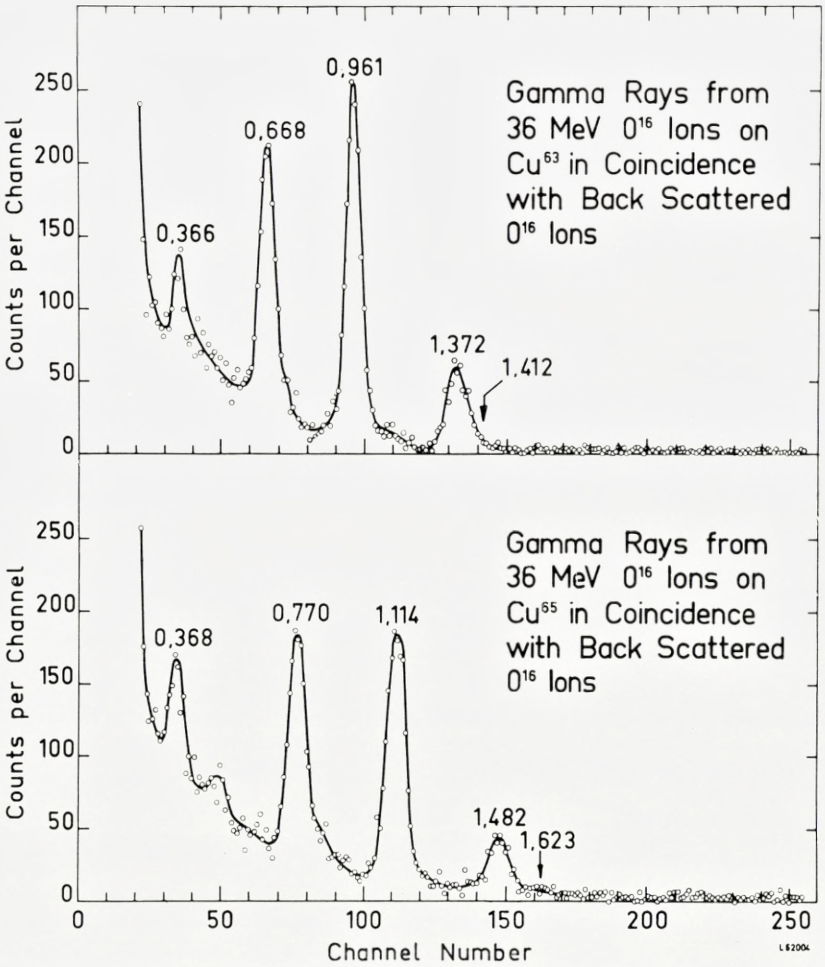

Fig. 8. Gamma ray spectra measured in coincidence with back scattered ions from 36 Mev O^{16} ions incident on thick separated targets of Cu^{63} and Cu^{65}.

employed). Since these levels are almost certainly 1/2− the gamma ray coincidence correlations will be spherically symmetric. Before these measurements, however, the gamma-ray spectra both direct and coincident with back scattered O^{16} ions were measured, using even larger solid angles than obtained from the 9 mm and 46 mm distances. (A solid angle of 5 % of a sphere for the particle counter and a distance of 30 mm for the gamma detector). The results for 36 Mev O^{16} ions on a thick natural copper target

are shown in Fig. 7 where both the direct and coincidence spectrum are displayed. The lack of linearity between energy and pulse height is attributed to the particular slow gate that was used. Coincidence spectra, using 36 Mev O^{16} ions and thick separated targets of Cu^{63} and Cu^{65}, are shown in Fig. 8.

Similar spectra to these, although with appreciably poorer statistics, were taken at 10° intervals from 0° to 90° in coincidence with back scattered ions, using both a thick unseparated target and a thick separated Cu^{65} target, at a bombarding energy of 36 Mev. The areas under the total absorption peaks of the 0.668, 0.961 and 1.327 Mev gamma rays in Cu^{63} and the 0.770, 1.114 and 1.482 Mev gamma rays in Cu^{65} were measured for the natural copper target, and for the latter three in the case of the separated Cu^{65} target. In the case of the separated Cu^{65} target the areas under the total absorption peaks could be readily estimated. Allowance was made for the pulses from 1.482 Mev gamma rays under both the 1.114 and 0.770 Mev peaks (see lower half of Fig. 8) and, since the intensity of 1.482 Mev gamma rays was low compared to the two lower energy gamma rays, uncertainties in this estimate are a small effect. A Zn^{65} source was used to get the line shape for 1.114 Mev gamma rays and, thus, to correct for pulses from these under the 0.770 Mev peak. In the case of the unseparated copper target a somewhat more arbitrary although reasonably reproducible scheme was used to get the peak areas. The dotted lines shown on the spectrum in the lower half of Fig. 7 were drawn and the peak areas above these lines were measured. This is, in fact, a reasonably good approximation to the true photopeak areas. Ratios to the area under the 0.668 Mev peak of the five other gamma peaks were then calculated for the natural target and to the 0.770 Mev peak for the 1.114 and 1.482 Mev peaks in the case of the Cu^{65} target. These were then fitted[21] by a least square procedure to a Legendre polynomial expansion given by equation (19), Appendix I, and the resulting coefficients for a_0 (from which the relative intensities can be calculated) are given in Table IV. As can be seen from the lower half of Fig. 7, it is difficult to estimate the area under the 1.482 Mev total absorption peak, even in the good statistics run on natural copper, so the intensity ratio of 1.482 Mev to 0.668 Mev gamma rays is not included in Table IV. The same comment applies to the ratio of 1.114 to 0.668 Mev gamma rays.

The values of the intensity ratios in Table IV obtained from the coefficient of P_0 in the least square fitting program plus the isotope ratio of Cu^{63} (69.1 %) and Cu^{65} (30.9 %) in natural copper permit relative yields of gamma rays per incident ion to be calculated for each of the three excited states of Cu^{63} and Cu^{65}, provided the relative total absorption peak efficiency

TABLE IV.

Relative peak intensities of gamma rays observed from 36 Mev O^{16} ions on thick targets of both natural copper and separated Cu^{65} in coincidence with back scattered ions. The results are averaged over angle.

Target	Gamma energy Mev	Isotope	Peak intensity
Copper	0.668	Cu^{63}	1.000
Copper	0.770	Cu^{65}	0.237 ± 0.008
Copper	0.961	Cu^{63}	1.190 ± 0.032
Copper	1.327	Cu^{63}	0.431 ± 0.011
Cu^{65}	0.770	Cu^{65}	1.000
Cu^{65}	1.114	Cu^{65}	1.170 ± 0.037
Cu^{65}	1.482	Cu^{65}	0.282 ± 0.007

of a 7.6 cm × 7.6 cm NaI(Tl) crystal at 46 mm distance is known as a function of the gamma-ray energy, and the branching ratios of the various levels are known. The total absorption peak efficiency was taken from curves of the total efficiency and of peak to total ratios[22]. As for the branching ratios, the only evidence for other than direct ground-state transitions is the presence of approximately 370 kev radiation observed in Figs. 7 and 8. Gamma-gamma coincidence experiments described below established that this radiation was in coincidence with 0.961 and 1.114 Mev gamma rays in Cu^{63} and Cu^{65}, respectively; no gamma-gamma coincidences between gamma rays of other energies were detected. The branching ratios of the 1.327 and 1.482 Mev levels were taken directly from the data of Fig. 8 where the solid angles of both particle and gamma counter were sufficiently large[1] so that no averaging over angle is necessary. The branching ratio for the 1.327 Mev level in Cu^{63} is 91 % by 1.327 Mev gamma rays and 9 % by 0.366 Mev gamma rays, and for the 1.482 Mev level in Cu^{65} it is 76 % by 1.482 Mev gamma rays and 24 % by 0.368 Mev gamma rays. These branching ratios, of course, must be used to correct both the observed intensities of 1.327 and 1.482 Mev gamma rays and also those of the 0.961 and 1.114 Mev gamma rays—part of whose yield results from the branching of the upper level. The experimentally determined relative gamma-ray intensities corrected for the various factors discussed above are listed in the last column of Table V. The third column in this table lists the thick target yields taken for 36 Mev O^{16} ions from Fig. 6, multiplied by $(2J + 1)$,

[1] The particle counter had a solid angle of about 5 % of a sphere and the gamma counter was 3 cm from the target center.

TABLE V.

Relative yields for various levels in Cu^{63} and Cu^{65}.

Level	J	$Y(2J+1)$ theory	Relative intensities (experimental)
0.668	1/2	1 (assumed)	1 (assumed)
0.961	5/2	1.58	1.60
1.327	7/2	0.835	0.918
1.862	(3/2)	0.106	≤ 0.021
0.770	1/2	1 (assumed)	1 (assumed)
1.114	5/2	1.34	1.49
1.482	7/2	0.723	0.699
1.623	(3/2)	0.253	< 0.050
0.668	1/2	1 (assumed)	1 (assumed)
0.770	1/2	0.801	0.766

where J is the spin of the excited state determined in the angular-correlation experiments described later and normalized to the value for the 0.668 and 0.770 Mev levels, respectively. To obtain relative values of $B(E2)$ it is merely necessary to divide the numbers in the last column by the corresponding numbers in the previous column and the results are tabulated in Table VI. The errors for the 0.961, 1.327 and 1.482 levels come from those calculated in the least square fitting procedure and listed in Table IV.

TABLE VI.

Relative values of $B(E2)$ for various levels in Cu^{63} and Cu^{65}.

Level (Mev)	Isotope	Spin	Relative $B(E2)\downarrow$
0.668	Cu^{63}	1/2	1.00
0.961		5/2	1.01 ± 0.03
1.327		7/2	1.10 ± 0.03
1.862		(3/2)	< 0.20
0.770	Cu^{65}	1/2	1.00
1.114		5/2	1.11 ± 0.04
1.482		7/2	0.97 ± 0.03
1.623		(3/2)	< 0.20
0.668	Cu^{63}	1/2	1.00
0.770	Cu^{65}	1/2	0.77 ± 0.03

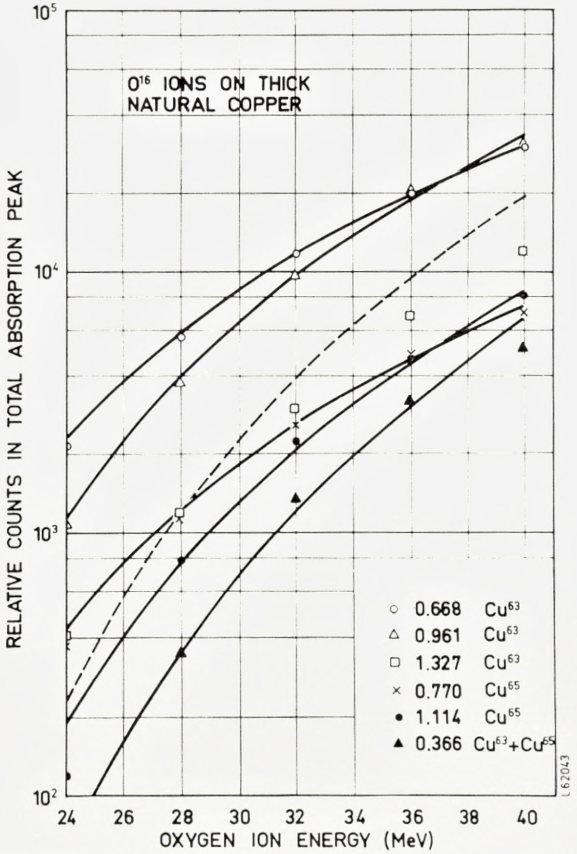

Fig. 9. Relative counts in the total absorption peak as a function of O^{16} ion energy of the six gamma-ray lines observed when a thick natural copper target is bombarded by O^{16} ions. Solid lines through the points are the best fits taken from the theoretical curves on Fig. 6.

The limits on the relative $B(E2)$ values listed in Tables V and VI for the 1.862 Mev level in Cu^{65} and the 1.623 Mev level in Cu^{65} were obtained from an analysis of the run shown in the lower half of Fig. 7 and another good statistics run taken later, also using a natural copper target. The upper limit on the intensities was obtained assuming the peaks to be less than half the intensity of the background at the place in the spectrum where the peaks would be expected to occur.

Absolute cross sections were measured with the apparatus shown in Fig. 3. In these experiments the direct gamma-ray spectrum from a thick natural copper target was measured at a number of O^{16} ion energies be-

TABLE VII.

Counts in photopeak for O^{16} ions on a thick natural copper target.

EO^{16}	E_γ	0.668	0.770	0.961	1.114	1.327	0.360
24		2.13 (3)	3.75 (2)	1.09 (3)	1.18 (2)	4.03 (2)	
28		5.60 (3)	1.14 (3)	3.78 (3)	7.82 (2)	1.19 (3)	3.51 (2)
32		1.16 (4)	2.61 (3)	9.71 (3)	2.23 (3)	2.98 (3)	1.35 (3)
36		1.99 (4)	4.86 (3)	2.03 (4)	4.74 (3)	6.78 (3)	3.24 (3)
40		2.98 (4)	6.97 (3)	3.07 (4)	8.05 (3)	1.20 (4)	5.18 (3)

tween 24 and 40 Mev. At each energy the counts in the photopeak of each gamma ray in the spectrum were measured by the technique previously described. These numbers are listed in Table VII and plotted in Fig. 9. The experimental points were then fitted by the theoretical yields from Fig. 6. The dotted curve in Fig. 9 is the theoretical yield from Coulomb excitation of the 1.327 Mev level in Cu^{63} and is seen to give rather bad agreement with the experimental points. The explanation is that a substantial fraction of the gamma rays of this energy actually arises from the reaction $C^{12}(O^{16},\alpha)Mg^{24}$ where the first excited state of Mg^{24} is strongly fed. The consequent 1.37 Mev gamma rays cannot be resolved from those due to copper. This emphasizes the importance of making measurements in coincidence with back scattered O^{16}, ions since these light element contamination reactions are peaked in both energy and intensity in the forward direction. The resulting improvement in the spectrum can be clearly seen in Fig. 7. The theoretical curve in Fig. 9 through the 0.366 Mev gamma-ray yield is that for the yield of a combination of 1.327 and 1.482 Mev gamma rays and is consistent with the fact that the 0.366 Mev gamma rays arise from cascades between the third and second excited states in the two isotopes.

The absolute yield for the 0.668 Mev level in Cu^{63} and the 0.770 Mev level in Cu^{65} were calculated from this data. The total charge collected during each run was measured by a calibrated beam integrator. The total absorption peak efficiency for a 7.6×7.6 cm NaI(Tl) counter at the distance of 5 mm (13 mm to the actual face of the NaI(Tl) crystal) used in these experiments was taken from the tables of HEATH[22]. An attenuation of 6 % for the material between the front face of the target and the surface of sodium iodide was estimated. The O^{16} beam employed was assumed to be in its charge V state as selected by the analyzing magnet. The results yielded absolute values of $B(E2)$ and these are listed in Table VIII. To check these results the same measurements were made on a thick natural iron target and the resulting values of $B(E2)$ are also given in Table VIII.

TABLE VIII.

Absolute values of $B(E2)\uparrow$ and $B(E2)\downarrow$ for the first excited state of Cu^{63}, Cu^{65} and Fe^{56}.

Target	E_γ(Mev)	Level $J\pi$		$B(E2)\uparrow$	$B(E2)\downarrow$
		Gnd	Exc		
Fe^{56}	0.845	0+	2+	0.097	0.019
Cu^{63}	0.668	3/2−	1/2−	0.0104	0.021
Cu^{65}	0.770	3/2−	1/2−	0.0078	0.015

b) Gamma-Gamma Coincidence Measurements

In this experiment the particle detector was replaced by a second 7.6 cm × 7.6 cm NaI(Tl) counter and coincidence spectra were measured in one gamma-ray detector with gates on the other set on various portions of the direct spectrum. The results are summarized in Fig. 10. The only coincidence observed both in the low energy portion of the spectrum (shown in Fig. 10) and the high energy part were those between 0.36 Mev gamma rays and 1.114 and 0.961 Mev gamma rays, respectively. A search was made to see whether any of the levels above 1.48 Mev decayed predominantly by cascade and hence explain the absence of direct transitions in the spectrum, but no evidence for such cascading was found. Having established, in this experiment, the origin of the 360 kev gamma rays the branching ratios of the third excited states in the two copper isotopes could be calculated from the data of Fig. 8, as described previously. It should be noted, in Fig. 10, that the peak at about 190 kev is due to Compton scattering from one crystal to the other and is highest when the voltage gate is set on the Compton edge of the 0.961 Mev gamma ray, that is on 770 kev pulses.

c) Particle-Gamma Angular Correlations

The results of the particle-gamma coincident angular correlation measurements, using the apparatus of Fig. 2 with $d = 15$ and $D = 58$ mm, normalized by the coincidence counts in a second fixed sodium iodide crystal are presented in Figs. 11, 12 and 13. Again, both thick natural copper targets and thick separated Cu^{65} targets were employed. To minimize contributions to the 1.327 Mev gamma peak from natural copper from the reaction $C^{12}(O^{16},\alpha)Mg^{24}$, $E_\gamma = 1.37$ Mev, the vertical position of the target was changed after each run. This was not possible in the case of the separated

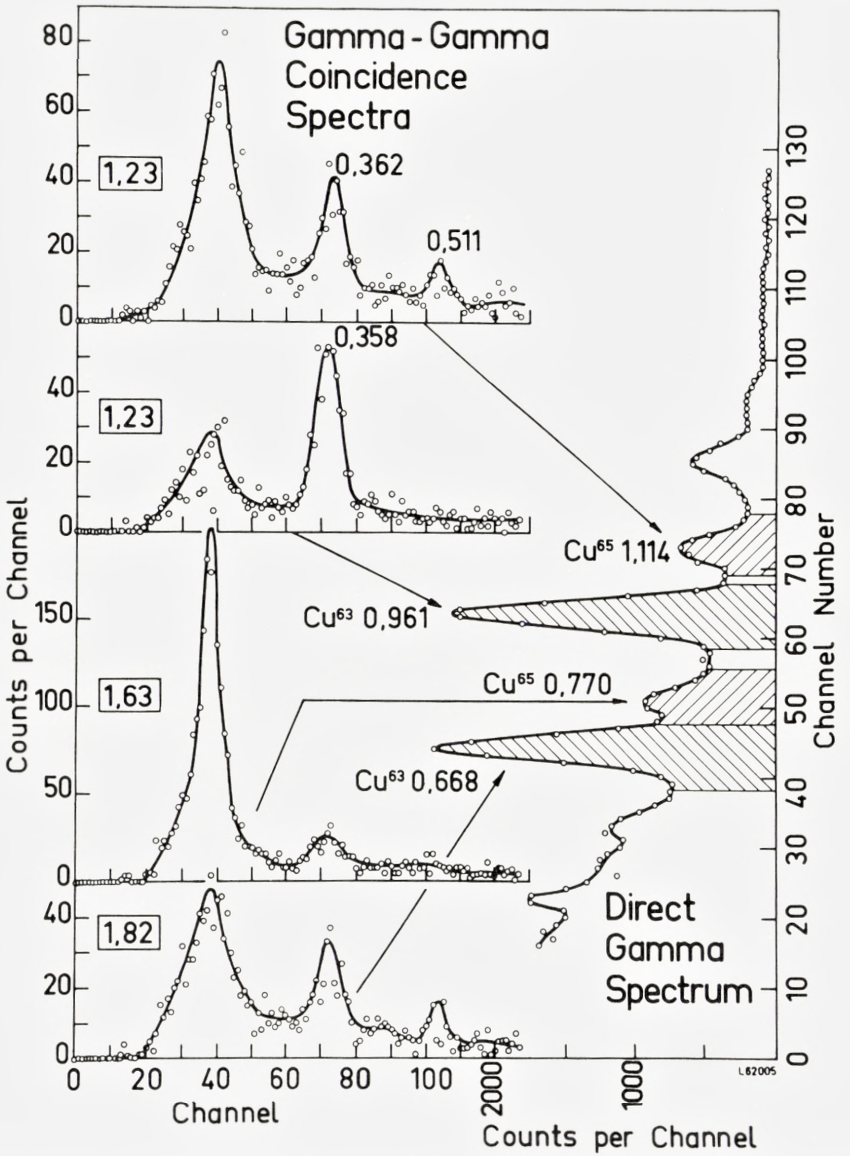

Fig. 10. Gamma-gamma coincidence measurements. The direct spectrum of gamma rays from 36 Mev O^{16} ions on a thick natural copper target is shown along the right side of the figure. Spectra in the second gamma-ray detector measured in coincidence with the respective gates (shown shaded on the direct spectrum) are shown on the left. The numbers in square boxes are proportional to the total gate counts in each case.

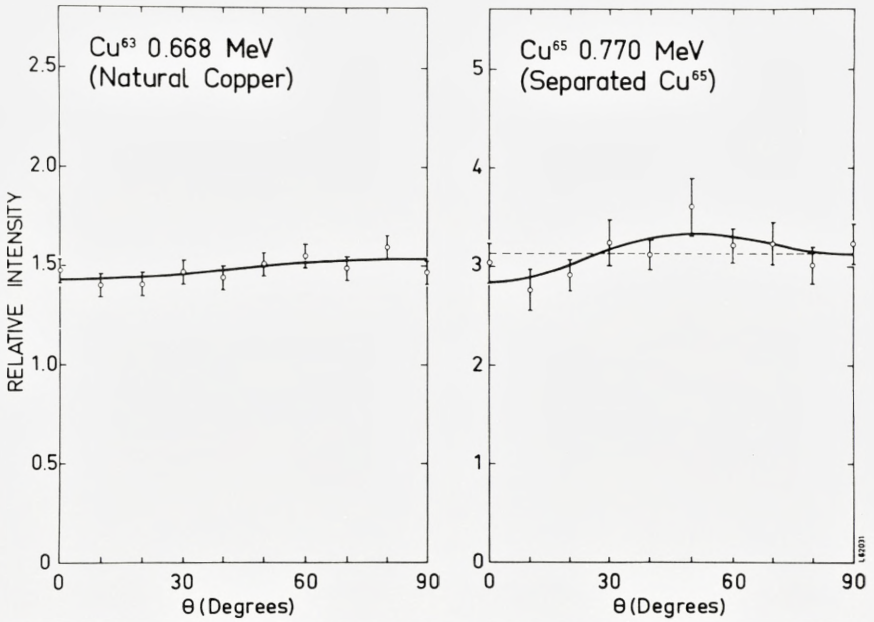

Fig. 11. Coincident angular correlations of 0.668 Mev gamma rays from a natural copper target and 0.770 Mev gamma rays from a separated Cu^{65} target normalized by coincident counts in the monitor gamma detector as described in the text. The solid curves are least square fits to a Legendre polynomial expansion. The dotted line is the average value of the intensity of 0.770 Mev gamma rays.

Cu^{65} target because of its small area. A pronounced 1.37 peak was observed in these spectra, which increased as a function of time as the carbon contamination built up on the target. Natural copper was used for measuring angular distributions of the 0.668, 0.961, 1.327 and 1.482 Mev gamma rays, while the separated Cu^{65} target gave the results for the 0.770 and 1.114 Mev gamma rays.

In both cases, background under each total absorption peak was estimated by drawing straight sloping lines as indicated on Fig. 7. In the case of the natural copper target, all pulses above about 550 kev in the coincident monitor spectrum were used to normalize the counts in each peak in the coincidence spectrum from the moving crystal at each angle. For the separated targets, however, the contamination gamma rays in the coincidence spectra prevented such an analysis; therefore, the counts in the total absorption peaks of 0.770 and 1.114 Mev gamma rays were used.

The six correlations were fitted by the method of least squares to the

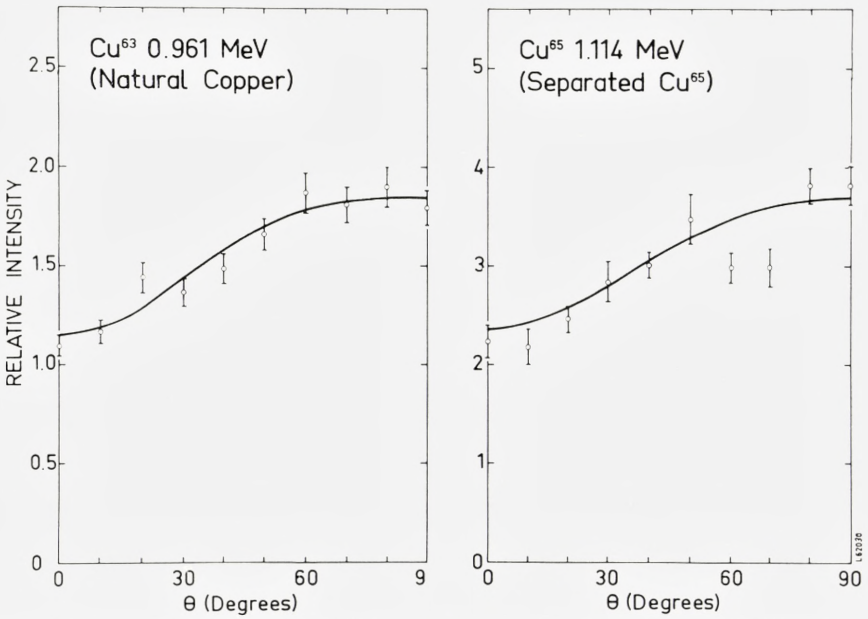

Fig. 12. Coincident angular correlations of 0.961 Mev gamma rays from a natural copper target and 1.114 Mev gamma rays from a separated Cu^{65} target. The solid curves are least square fits to a Legendre polynomial expansion.

TABLE IX.

Legendre polynomial coefficients obtained from a least square analysis of coincident angular correlation data on natural copper and separated Cu^{65} targets.

Level energy Mev	Isotope	Target	a_2/a	a_4/a_0
0.668	Cu^{63}	Copper	-0.045 ± 0.026	-0.004 ± 0.032
0.770	Cu^{65}	Cu^{65}	-0.015 ± 0.046	-0.100 ± 0.055
0.961	Cu^{63}	Copper	-0.242 ± 0.026	-0.080 ± 0.031
1.114	Cu^{65}	Cu^{65}	-0.252 ± 0.040	-0.040 ± 0.047
1.327	Cu^{63}	Copper	$+0.240 \pm 0.330$	-0.072 ± 0.039
1.482	Cu^{65}	Copper	$+0.250 \pm 0.079$	$+0.016 \pm 0.094$

$$W(\theta) = 1 + (a_2/a_0)P_2(\cos\theta) + (a_4/a_0)P_4(\cos\theta)$$

Theory 3/2−7/2−3/2 +0.36 −0.09

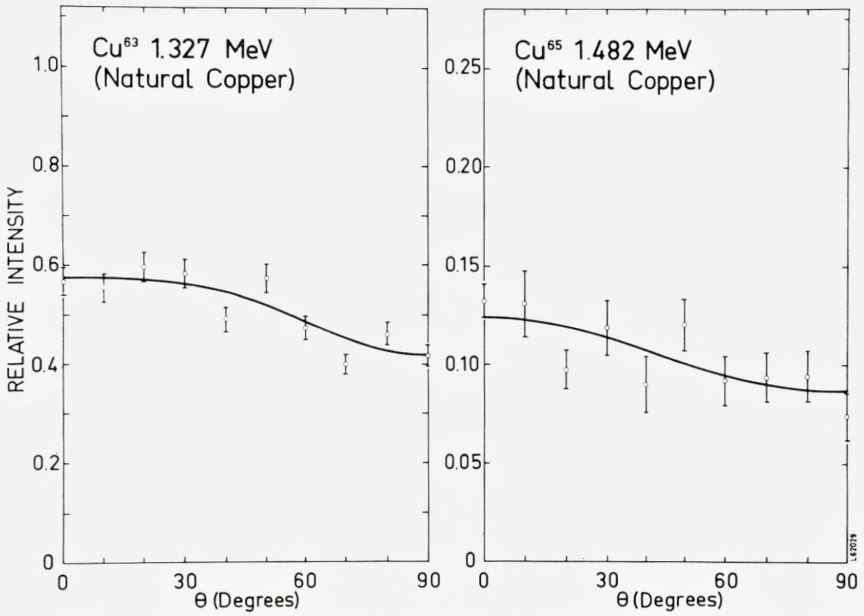

Fig. 13. Coincident angular correlations of 1.327 and 1.482 Mev gamma rays from a natural copper target. The solid curves are least square fits to a Legendre polynomial expansion.

Legendre polynomial expansion given by equation (19) in Appendix I, and the values are listed in Table IX. The errors on each coefficient were calculated from the average statistical error on the points in each distribution. The resulting Legendre polynomial expansions are plotted as solid lines in Figs. 11 to 13.

5. Discussion of Experimental Results

In this experiment it has been possible to excite with certainty, by the Coulomb excitation process, three levels in both Cu^{63} and Cu^{65}. There is no evidence that the level at 1.86 Mev is excited in Cu^{63}, and a lower limit has been placed on its $B(E2)$. There is no evidence either for Coulomb excitation of the known fourth excited state in either nucleus, and in the case of Cu^{65} a lower limit has been placed on its $B(E2)$. In each nucleus the three levels excited have equal values of $B(E2)\downarrow$ within a few percent.

The absolute value of $B(E2) = 0.097 \times e^2 \times 10^{-48}$ cm^4 measured for the 0.845 Mev level in Fe^{56} is in good agreement with previous values of 0.10 by Temmer and Heydenburg[9], 0.10 by Broude and Gove[23], and

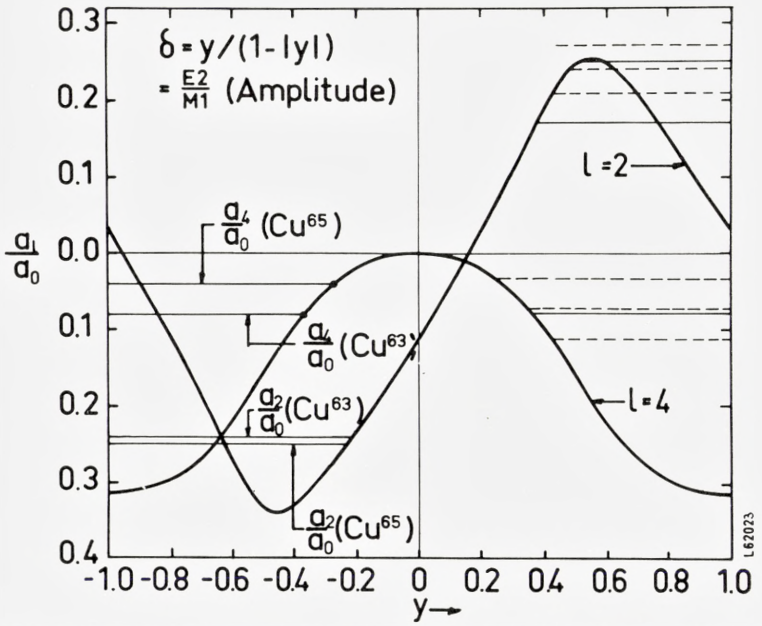

Fig. 14. a_2/a_0 and a_4/a_0 vs. y for the case of $E2$ Coulomb excitation of a state of spin 3/2 to a state of spin 5/2 with subsequent decay by an $E2$–$M1$ mixture. These angular correlation coefficients are calculated for the particular geometry employed in the present experiments. The experimentally determined values for the 0.961 Mev level in Cu^{63} and the 1.114 Mev levels in Cu^{65} are shown.

$0.100 \pm .025$ by Eccleshall, Adams and Yates[24]. It is about 40 % higher than the value of 0.07 obtained by Alkazov et al.[25]. The present results for the copper isotopes are not in good agreement with recent measurements by Yerohkina and Lemberg[26], using 36 Mev N^{14} ions, who obtain values which are between 30 and 50 % higher than those reported here. In the present measurements the ratio of $B(E2)$ for the 0.668 Mev level in C^{63} to $B(E2)$ for the 0.845 Mev level in Fe^{56} is a particularly accurate experimental number, since it is independent of a knowledge of the absolute beam current or absolute gamma counter efficiency. The measured ratio is 1.075 ± 0.010.

The yield curves as a function of O^{16} ion energy shown in Fig. 9 agree reasonably well with $E2$ Coulomb excitation theory up to 40 Mev, despite the fact that this must be very close to the barrier. This implies, in particular, that the theoretical expressions for the angular correlations given by Alder et al.[11] can be used with confidence in analyzing the angular distribution

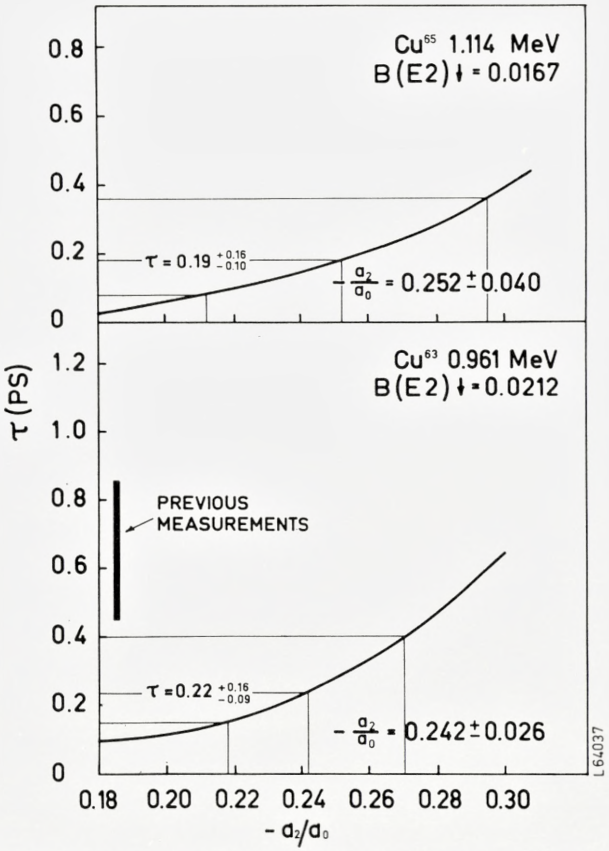

Fig. 15. The mean lifetime τ in picoseconds for the 0.961 Mev level in Cu^{63} (lower half) and the 1.114 Mev level in Cu^{65} (upper half) plotted as a function of a_2/a_0, where a_2/a_0 is the coefficient of $P_2(\cos\theta)$ in the theoretical expression for the coincidence angular correlation measured in the geometry used in the present experiments. In deriving these relationships the measured values of $B(E2)$ given on the figure were used. Experimentally measured values of a_2/a_0 and hence of τ are shown. The vertical black bar shows the range of values determined by others.

results, at least as far as first-order effects are concerned. Second-order effects are discussed in Appendix II, where they are shown to be negligible.

It can be concluded with considerable certainty that the three ground-state gamma-ray transitions observed in both Cu^{63} and Cu^{65}, when these isotopes are bombarded with O^{16} ions, can arise as a result of electric quadrupole Coulomb excitation. Hence, their spins and parities must be 1/2-, 3/2-, 5/2- or 7/2-. For both the case of spin 1/2 and spin 3/2 the gamma-gamma angular correlation coefficients $A_2^{(2)}$ and $A_4^{(2)}$ vanish, in the first

case for obvious reasons and in the second because of an accidental vanishing of the Racah coefficient $W(2,3/2,\ 2,3/2;\ 3/2,\ 2)$. For spin 7/2 the angular correlation is unique, because the de-excitation gamma rays must be pure $E2$. For spin 5/2 the angular correlations depend on δ, the $E2$ to $M1$ amplitude mixture of the de-excitation gamma rays.

The coincidence angular correlations of 845 kev gamma rays from $Fe^{56}(O^{16}, O^{16\prime}\gamma)$ following Coulomb excitation by 33 Mev O^{16} ions agree with the theoretical prediction for a 0–2–0 situation and, in particular, demonstrate that coefficients of $P_4(\cos\theta)$ in the angular correlations are only attenuated by about a factor of 3 over what they would be for a point-particle counter at 180° and a point-gamma counter. Severe though this factor may appear it still permits a_4 coefficients to be measured with sufficient precision to make spin assignments and to measure $E2$–$M1$ mixtures.

The angular correlations for the three levels in Cu^{63} and Cu^{65} are shown in Figs. 11, 12 and 13, and results of the least square fits are listed in Table VIII. For both the 0.668 Mev level in Cu^{63} and the 0.770 Mev level in Cu^{65} the correlations are spherically symmetric within the counting statistics. This is consistent with spin assignments of 1/2- or 3/2- for the levels and, in fact, can even be fitted by a spin of 5/2-, provided an appropriate value of the $E2$–$M1$ mixing is chosen. This can be seen by referring to Fig. 14, where the theoretical predictions for a_2/a_0 and a_4/a_0 obtained from equations (19) and (20) in Appendix I are plotted as a function of y, where y is related to the $E2$–$M1$ amplitude ratio δ as follows

$$\delta = \frac{y}{1 - |y|}. \tag{7}$$

For a value of $y = 0.15$, both a_2/a_0 and a_4/a_0 are essentially zero. However, on the basis of other evidence, a spin assignment of 1/2- is almost certain for both levels. A discussion of this assignment has been given by Cumming et al.[27]).

Of the four possible spin assignments, the only one which can result in a negative a_2/a_0 term in the distribution is 5/2-, since the predicted distribution for the geometry used in this experiment for a spin of 7/2- is

$$W(\theta) = 1 + 0.36P_2(\cos\theta) - 0.09P_4(\cos\theta). \tag{8}$$

Hence, the 0.961 Mev level in Cu^{63} and the 1.114 Mev level in Cu^{65} have both spin and parity 5/2-. The small a_4/a_0 term observed, in both cases,

removes the ambiguity of the double value of a_2/a_0 and allows a unique assignment of the $E2$–$M1$ amplitude ratio δ (see Fig. 14). The values of δ are, respectively, -0.21 ± 0.08 for the .961 Mev level in Cu^{63} and -0.24 ± 0.13 for the 1.114 Mev level in Cu^{65}. The former value is somewhat smaller than the value of $\delta^2 = 0.16$ measured by CUMMING et al.[27].

The angular correlations of both the 1.327 Mev gamma rays from Cu^{63} and 1.482 Mev gamma rays from Cu^{65} have large positive a_2/a_0 coefficients. Reference to Fig. 14 shows that this is not consistent with a 5/2 spin assignment since, for the observed values of a_2/a_0, one would expect values of a_4/a_0 in the vicinity of -0.2. The only other possible assignment then is 7/2-, and the theoretical expression for this is given above. Both the experimental distributions have smaller values of a_2/a_0 than predicted theoretically although, in the case of the 1.482 Mev gamma rays, the experimental uncertainty virtually includes the theoretical value. A number of possible explanations for this discrepancy have been considered and found to be unsatisfactory. It cannot be due to a ξ dependence of the coefficients since this has been shown to be negligibly small. It cannot be due, in the case of the 1.327 Mev gamma ray in Cu^{63}, to the presence of 1.37 Mev gamma rays from $C^{12}(O^{16},\alpha)Mg^{24}$ since the 0-2-0 nature of the latter's angular distribution would have the effect of making a_2/a_0 larger and also of introducing a large negative P_4 term. It is unlikely that any higher levels in either isotope are excited and subsequently decay through the 1.327 or 1.482 Mev levels. Finally, it cannot be due to second-order effects as discussed in Appendix II. Despite the discrepancy, it is concluded that both the 1.327 and 1.482 Mev levels have spin and parity 7/2-.

The combined measurements of $B(E2)$ and δ for the 0.961 and 1.114 Mev levels in Cu^{63} and Cu^{65}, respectively, allow the lifetimes of these two levels to be estimated. Using the measured values of $B(E2)$, a plot of lifetime vs a_2/a_0, the coefficient of $P_2(\cos\theta)$ in the angular distribution can be made and such plots are shown in Fig. 15. The resulting values of the mean lifetime from the measured values of $B(E2)$ and a_2/a_0 obtained in this experiment are $0.19\ ^{+0.16}_{-0.10}$ ps for the 1.114 Mev level in Cu^{65} and $0.22\ ^{+0.16}_{-0.09}$ ps for the 0.961 Mev level in Cu^{63}. Several previous measurements have been made for the latter level[27, 28, 29, 30] from which an average value of 0.645 ± 0.2 ps has been estimated. The present measurement is in reasonable agreement considering the indirect method involved.

6. Conclusions and Comparison with Theory

The results of the present experiment as shown in Fig. 16 establish that the spins of the second and third excited states in Cu^{63} and Cu^{65} are 5/2 and 7/2, respectively. In both cases, the measurements are consistent with a spin of 1/2 for the first excited state, and this assignment is also consistent with other measurements. Since the Coulomb excitation is almost certainly electric quadrupole, the parities of all three excited states in both nuclei are the same as the ground state. In both cases, the third excited state branches to the second as well as decaying directly to ground and the second excited state has an $E2$ to $M1$ amplitude mixture in its ground state transition of $\delta = -0.2$. This amplitude ratio with its associated uncertainty obtained from Fig. 14, when combined with the measured values of the absolute $B(E2)$, yield retardation factors over the Weisskopf unit[31] in the range from 7 to 20 for the $M1$ part of the 0.961 Mev radiation in Cu^{63} and in the range from 6–29 for the $M1$ part of the 1.114 Mev radiation in Cu^{65}.

The values of $B(E2)$ for each of the three levels in Cu^{63} are the same within the experimental uncertainty and this is true too for Cu^{65}. The absolute values of $B(E2)$ are also quite similar to those for the adjacent even-even nuclei Ni^{62} and Ni^{64} [32] as well as for Ni^{58} and Ni^{60} [32, 23].

As discussed in the introduction, there are several reasons why the weak-coupling picture is not appropriate. The observation of an $M1$ component in the decay between the 5/2-- state and the ground state is also in disagreement with this model. A detailed comparison of the present and other data with the predictions of various models proposed to explain the properties of odd-A nuclei has been given elsewhere[33].

There is no evidence in the present experiments for the missing 3/2- excited state in either Cu^{63} or Cu^{65}. This is in contrast with recent work on the elastic scattering of 43 Mev alpha particles from Cu^{63} and Cu^{65} [35]. In Cu^{63}, for example, the 1.862 Mev level is excited and possibly the level at 1.547 Mev. In the case of the 1.862 Mev level the intensity is such as to indicate a $B(E2)$, which is 0.3 ± 0.07 times the average of the $B(E2)$ for the first three excited states. The measurements reported here indicate that the factor is less than 0.2. Similar results from the alpha-scattering experiments are found for Cu^{65}.

The splitting in energy between members of the quartet of levels formed by coupling a $p_{3/2}$ proton to the 2+ core state arises from the interaction between this odd particle and the core. This interaction can be written as a multipole expansion of the product of two tensors of degree r, one of

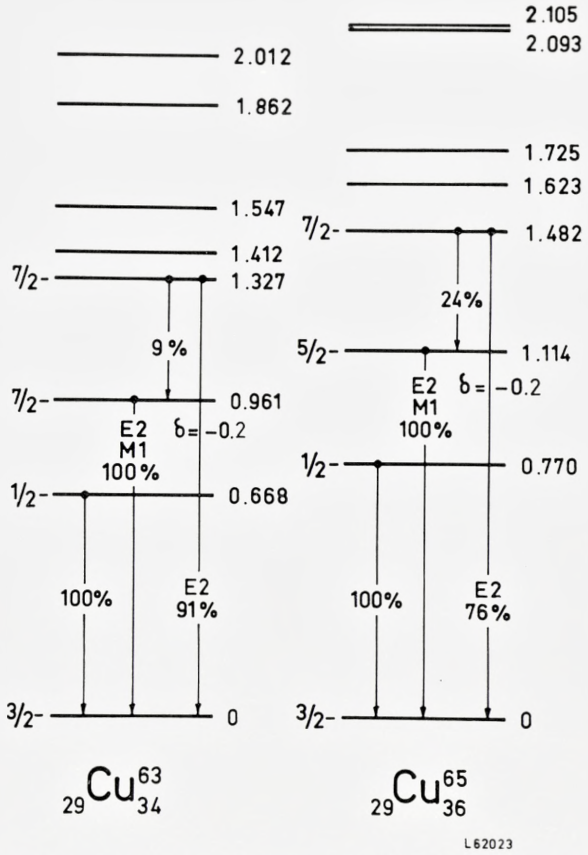

Fig. 16. Level diagrams for low lying states in Cu^{63} and Cu^{65}.

which operates on the core degrees of freedom and the other on the degrees of freedom of the particle. The tensorial degree r, in this case, can have values from 0 to 3, being limited by twice the spin of the odd particle. Such expansions yield a set of four spectra associated with monopole, dipole, quadrupole and octupole interactions between the particle and core, the sum of which gives the observed spectra. This expansion has been carried out[36] for Cu^{63} and Cu^{65}, assuming that the 3/2- state is at 1.412 and 1.623 Mev, respectively, in the two nuclei; the results are shown in Fig. 17. In both cases, a large positive octupole interaction is indicated with a smaller positive dipole and an almost negligible positive quadrupole. The monopole—or center-of-gravity position for Cu^{63} deviates from that of the 2 +

state in Ni^{62} by only 4 kev in 1.172 Mev and for Cu^{65} by 11 kev in 1.34 Mev. If, on the other hand, one assumes that the 3/2- level in Cu^{63} is at 1.86 Mev, an even larger positive octupole, the same very small positive quadrupole, and a negligible dipole term are obtained. In fact, to an excellent approximation, a positive octupole term alone reproduces the spectrum rather exactly. The center of gravity now, however, deviates from that in Ni^{62} by 87 kev. Similar results would be obtained for Cu^{65} if the 3/2- level were assumed to be near 2 Mev excitation.

The dominance of an octupole term in both copper isotopes for the particle-core interaction is rather surprising. It is not compatible, for example, with a naive model of the copper nuclides in which one assumes the $p_{3/2}$ neutron shell and the $f_{7/2}$ proton shell is really closed and describes Cu^{63} as a $p_{3/2}$ proton coupled to two neutrons in the $f_{5/2}$ shell and Cu^{65} as a $p_{3/2}$ proton coupled to two holes in the $f_{5/2}$ neutron shell. In this case, the two are identical except that the quadrupole level sequence will be inverted. In fact, if the interaction is exclusively between the $p_{3/2}$ shell (for protons) and the $f_{5/2}$ shell (for neutrons), then Nordheim's number is even and the interaction is expected to have a large quadrupole term, a smaller dipole term, and a negligible octupole term[37]. If, however, the odd particle, no matter what its configuration may be, is coupled to vibrational levels in the core, then the quadrupole part of the multipole expansion will vanish simply because it is proportional to the quadrupole moment of the vibrational state, and this is zero. One can therefore conclude that the negligible quadrupole contribution in both the copper isotopes is evidence for the fact that the 2+ excited state of the appropriate nickel isotope is a vibrational state. A multipole expansion of the levels in Au^{197} was also carried out and a rather small quadrupole contribution was found, which again supports the assumption that one is dealing with a vibrational core.

In conclusion, one might say that the low lying levels of the copper isotopes show many of the features expected from the coupling of a single particle to a vibrating core. It is remarkable that the equality of the reduced transition probability for decay of the three lowest levels is preserved in spite of heavy mixing with other single-particle levels. This mixing is evidenced by the level splittings but maybe is most clearly seen from the recent stripping experiments[5].

Whereas the Coulomb excitation mainly measures the collective part of the wave function, the stripping experiments measure the single-particle contribution to the nuclear states. It seems possible in this way to obtain an experimental set of expansion coefficients which ought to give a consistent picture of the properties of these nuclei.

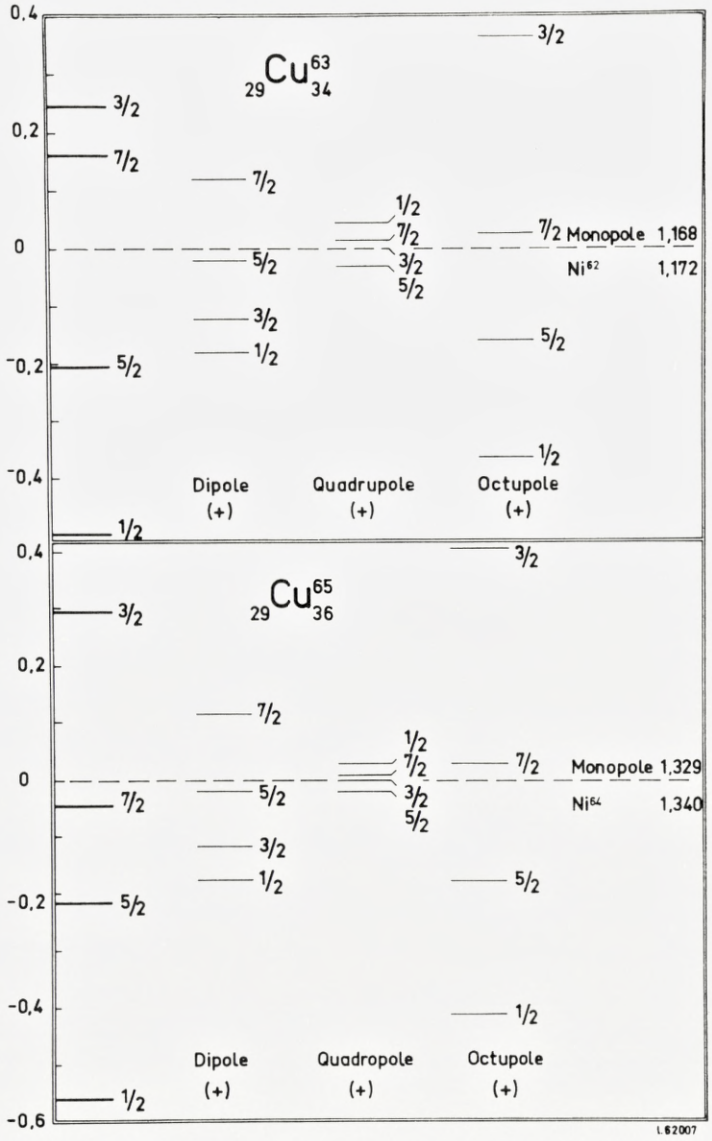

Fig. 17. Multipole expansion of the particle-core interaction in Cu^{63} and Cu^{65} if the missing 3/2-level is at 1.412 and 1.623 Mev, respectively.

7. Acknowledgement

It is a pleasure to acknowledge the many informative discussions on aspects of the experimental work with O. Nathan and Y. Yoshizawa and on the theoretical interpretation with A. Bohr, J. B. French, M. Harvey, E. Vogt and D. Beder. One of us (HEG) expresses his sincere appreciation to the Institute for Theoretical Physics, University of Copenhagen, for the hospitality extended to him during his one year's stay there.

Appendix I

a) Theoretical Angular Distributions

In a pure $E2$ Coulomb excitation process the coincidence angular correlation between a gamma counter moving in a plane and making angles θ with respect to the incident beam and a particle counter fixed at 180° to the beam (assuming point counters in both cases) is given by[11]

$$W(\theta) = 1 + 2A_2^{(2)}P_2(\cos\theta) - 1.5A_4^{(2)}P_4(\cos\theta), \tag{9}$$

where $A_2^{(2)}$ and $A_4^{(2)}$ are tabulated[11] gamma-gamma angular correlation functions. On the other hand, if only the direct angular distribution of the gamma rays is measured following $E2$ Coulomb excitation, the angular correlation in the classical limit is given by

$$W(\theta) = 1 + 0.5A_2^{(2)}P_2(\cos\theta) + 0.01A_4^{(2)}P_4(\cos\theta). \tag{10}$$

In this latter case, the coefficients actually depend on the parameter ξ[11] and equation (10) applies when $\xi = 0.3$. In the former case, not only is there no ξ dependence, but the correlations are much more asymmetric, in particular the coefficient of P_4 is very much larger, making it easier to measure multipole mixing in the de-excitation gamma radiation. It should be emphasized that, in the derivation of the above expressions, it has been assumed that the reaction mechanism is pure first order $E2$ Coulomb excitation in the classical limit, and this assumption is justified in the case of the present experiment, as shown in Appendix II.

Litherland and Ferguson[17] have derived a more general expression for the angular correlation of gamma rays arising from a particle-in particle-out reaction in the case when the gamma rays are detected in coincidence with the outgoing particle measured at either 0° or 180° to the incoming particle beam. Their expression is parameterized in terms of the relative

populations of magnetic substates of the level emitting the gamma ray. The gamma ray angular distribution is given by the following expression:

$$W(\theta) = \sum_{P_1 m_{f_1} k} (-1)^r P(m_f) \delta^p (I_f I_f m_f - m_f \mid k0) Z_1(LI_f L' I_f, I_i k) P_k(\cos\theta), \quad (11)$$

where I_f and m_f are the total angular momentum and its projection along some axis (in this case the beam direction) of the state emitting the gamma radiation, I_i is the total angular momentum of the nucleus after the gamma ray is emitted, $P(m_f)$ is the population of the magnetic substate m_f, δ is the amplitude mixing ratio of quadrupole to dipole radiation ($p = 0$ for $LL' = 11$, $p = 1$ for $LL' = 12$ and $p = 2$ for $LL' = 22$; the term with $LL' = 12$ has an additional factor of 2); Z_1 is a coefficient tabulated by SHARP et al.[38] $P_k(\cos\theta)$ is the Legendre polynomial and $r = J_i + m_f + L + L' + k/2$.

In equation (11), one normally regards the magnetic substate populations as parameters to be determined experimentally since they depend on the mechanism of the reaction used to populate them. In the case of Coulomb excitation, of course, the reaction mechanism is known and the magnetic substate populations can be calculated. The incoming and outgoing particles are directed along the z-axis and no change in the quantum number of the magnetic substate can occur. If the Coulomb excitation is by an electric quadrupole transition, then $E2$ transitions can only connect initial and final states having the same magnetic quantum number, and the population $P_f(m_i)$ of a final state with magnetic quantum number m_i is related to the population $P_i(m_i)$ of the initial state with magnetic quantum number m_i by the relation

$$P_f(m_i) = P_i(m_i)(I_i 2 m_i 0 \mid I_f m_i)^2. \quad (12)$$

It can readily be shown that inserting equation (12) into (11) results in the same expression as given in equation (9), since, in the ground state, all the magnetic substates are equally populated.

Again, because the reaction mechanism is known in the case of Coulomb excitation, it becomes possible readily to calculate the angular correlation to be expected when particle counters of finite solid angle are used, and this is discussed in the following section.

b) Corrections for Finite Solid Angle of Particle Detectors

A general expression for the coincidence angular correlations between inelastically scattered particles and gamma rays following Coulomb excitation has been given by ALDER et al.[11]. It can be written as follows:

$$W(\theta,\varphi,\theta_\gamma,\varphi_\gamma) = \sum_{k,\varkappa} b^{\lambda}_{k\varkappa}(\theta,\varphi,\xi) A_k^{(\lambda)} Y_{k\varkappa}(\theta_\gamma,\varphi_\gamma), \tag{13}$$

where the parameter ξ on which the cross section depends rather sensitively is given explicitly by ALDER et al.[11], $A_k^{(\lambda)}$ is the tabulated gamma-gamma correlation function[11], $Y_{k\varkappa}(\theta,\varphi)$ are the normalized spherical harmonics[39, 17], and the formula for the $b^{\lambda}_{k\varkappa}(\theta,\varphi,\xi)$ is given[11] for electric Coulomb excitation in a frame of reference in which the incident beam direction is taken as the z-axis; θ, φ, θ_γ, φ_γ, are the polar and azimuthal angles, respectively, of the particle and gamma counter. Since the plane in which the gamma counter moves can be defined as the zero for azimuthal angles, one can let $\varphi_\gamma = 0$. Furthermore, because the gamma counters have azimuthal symmetry, finite solid angle corrections may be introduced by inserting a factor Q_k in equation (13). If all pulses in the gamma-ray spectrum are counted at each angle these attenuation factors Q_k for a 7.6×7.6 cm NaI(Tl) counter may be obtained from the tables of RUTLEDGE[18].

Equation (13) is rather complicated in the general case, but considerable simplifications occur if the particle-counter geometry is chosen correctly. For example, all terms with $\varkappa$ = odd can be eliminated in a number of different geometries, viz:

1. An annular counter through which the beam passes
2. Two-particle counters $\theta_1 = \theta_2$, $\varphi_1 = \varphi$, $\varphi_2 = \varphi + 180^\circ$
3. Three-particle counters $\theta_1 = \theta_2 = \theta_3$, $\varphi_1 = 0$, $\varphi_2 = 120^\circ$, $\varphi_3 = 240^\circ$
4. Four-particle counters $\theta_1 = \theta_2 = \theta_3 = \theta_4$, $\varphi_1 = 0^\circ$, $\varphi_2 = 90^\circ$, $\varphi_3 = 180^\circ$, $\varphi_4 = 270^\circ$
5. Five-particle counters all at the same θ and equally spaced in φ with $\varphi_1 = 0$.

The elimination of odd $\varkappa$ has the advantage that the resulting expression for the angular correlation can be expanded in ordinary Legendre polynomials.

In these cases, the angular correlation expression (equation 13) is the following[40]:

$$\left.\begin{aligned} W(\theta,\varphi,\theta_\gamma) &= A + A_2^{(2)} Q_2 (C + 6D\cos(\pi+\theta) P_2^0(\cos\theta_\gamma) \\ &+ 1/2\cos 2\varphi(2D\cos(\pi+\theta) - C) P_2^2(\cos\theta_\gamma) - A_4^{(2)} Q_4 \\ &3/32\{(3B + 20D\cos(\pi+\theta) + 70E\cos 2(\pi+\theta)) P_4(\cos\theta_\gamma) \\ &- 1/3\cos 2\varphi(B + 4D\cos(\pi+\theta) - 14E\cos 2(\pi+\theta) P_4^2(\cos\theta_\gamma) \\ &+ 1/24\cos 4\varphi(B - 4D\cos(\pi+\theta) + 2E\cos 2(\pi+\theta) P_4^4(\cos\theta_\gamma)\}, \end{aligned}\right\} \tag{14}$$

where the quantities A, B, C, D and E are functions of $I_{2\mu}(\theta,\xi)$, the classical orbital integrals for $E2$ Coulomb excitation[11] as follows:

$$\left.\begin{aligned} A &= 2I_{20}I_{20} + 3(I_{22}I_{22} + I_{2-2}I_{2-2}) \\ B &= 4I_{20}I_{20} + I_{22}I_{22} + I_{2-2}I_{2-2} \\ C &= -2I_{20}I_{20} + 3(I_{22}I_{22} + I_{2-2}I_{2-2}) \\ D &= I_{20}I_{22} + I_{20}I_{2-2} \\ E &= I_{22}I_{2-2}. \end{aligned}\right\} \quad (15)$$

It can readily be shown that, when $\theta = 180°$, equation (14) reduces to equation (9). In the case of an annular counter the above expression becomes independent of φ and has the following relatively simple form:

$$\left.\begin{aligned} W(\theta,\theta_\gamma) &= 1 + A_2^{(2)}Q_2\left\{\frac{6D\cos(\pi+\theta)+C}{A}\right\}P_2(\cos\theta_\gamma) - 3/32 \\ & A_4^{(2)}Q_4\left\{\frac{3B+20D\cos(\pi+\theta)+70E\cos 2(\pi+\theta)}{A}\right\}P_4(\cos\theta_\gamma), \end{aligned}\right\} \quad (16)$$

where the quantities in curly brackets are functions of both θ and ξ and can be readily evaluated by graphical or numerical integration for any dimensions of an annular counter. The dependence of these quantities on θ for an annular counter with a mean angle equal to that of the counter used in the present experiment is discussed below.

The counter geometry used in the present experiments does not resemble any of the geometries listed above, except in that terms in equation (13) with $\varkappa$ odd are eliminated and hence equation (14) applies. This is always true if the counter is symmetric about the plane in which the gamma counter is moved. It is therefore necessary to perform some sort of numerical integration over the counter area. In the present work, this was done by dividing the area of each counter into six equal areas, calculating the angular distribution for each according to equation (14), weighting each by the relative solid angles and then adding the six distributions together. For a counter of the dimensions shown in Fig. 2, when the distance d between counter and target is 9 mm, the angular correlation is given by

$$\left.\begin{aligned} W(\theta_\gamma) = 1 &+ A_2^{(2)}Q_2(1.70P_2^0 + 0.0269P_2^2) - A_4^{(2)}(0.843P_4^0 \\ &+ 0.0171P_4^2 - 0.428\times 10^{-5}P_4^4). \end{aligned}\right\} \quad (17)$$

The P_l^ms, of course, are all functions of $\cos\theta_\gamma$.

The term in P_4^4 is negligible here and also for the case when d is 15 mm where the correlation becomes

$$\left.\begin{aligned} W(\theta_\gamma) = 1 + A_2^{(2)}Q_2(1.86P_2^0 + 0.0133P_2^2) - A_4^{(2)}Q_4 \\ (1.16P_4^0 + 0.00915P_4^2). \end{aligned}\right\} \quad (18)$$

Since both equations (17) and (18) have been calculated for $\xi = 0.3$, it is necessary to inquire whether the calculated coefficients are seriously dependent on ξ. It is known, for example, that for the direct gamma correlations the coefficients in equation (10) are very strongly dependent[11]. In order to answer this question readily, calculations were made for an annular counter with the same mean angle θ as for the counters employed in this experiment. This mean angle for the second geometry is 155°. Using this angle the coefficients in curly brackets in equation (16) which will be designated as a_2 and a_4, respectively, were evaluated for ξ in the range 0 to 1. Over this extensive range a_2 varied from 1.87 to 1.82 and a_4 from 1.18 to 1.08. It should be noted, incidentally, that the values at $\xi = 0.3$ are identical to the coefficients of P_2^0 and P_4^0, respectively, in equation (18), which indicates that the geometry employed is a rather good approximation to an annulus. Of course, for a counter exactly at 180°, there is no ξ-dependence and the above calculation demonstrates that even for angles up to 155° the ξ-dependence is negligible. This is a very considerable advantage of the correlation technique in which coincidences are taken with back scattered ions as opposed to measurements of the direct gamma-ray angular distributions.

These expressions have the unfortunate feature that it is difficult directly to compare them with experiment since the experimental data is fitted to a Legendre polynomial expansion of the form

$$W(\theta_\gamma) = a_0 + a_2P_2(\cos\theta_\gamma) + a_4P_4(\cos\theta_\gamma), \quad (19)$$

particularly when the radiation is mixed dipole-quadrupole. They can, however, be reduced to this form where, of course, both the coefficients a_0 and a_2 will be functions of $A_2^{(2)}Q_2$ and $A_4^{(2)}Q_4$. For a particle counter distance of 15 mm the expression becomes

$$\left.\begin{aligned} 1 + 0.03A_4^{(2)}Q_2 - 0.019A_4^{(2)}Q_4 + (1.83A_2^{(2)}Q_2 - 0.093A_4^{(2)}Q_4)P_2^0 \\ - 1.05A_4^{(2)}Q_4P_4^0. \end{aligned}\right\} \quad (20)$$

Appendix II

Second-Order Coulomb Excitation Effects

Because the relative $B(E2)$ for the three levels in Cu^{63} and Cu^{65} were obtained from gamma-ray spectra measured in coincidence with back scattered O^{16} ions detected in a counter near 180°, it is necessary to estimate how the results might be changed by second-order Coulomb excitation effects. Such effects are known to have their maximum values in this geometry and with heavy bombarding ions. Recently, BEDER[41] has written a computer program for calculating second-order Coulomb excitation cross sections and has shown that, in certain circumstances, the interference term between first and second order can be quite large.

The situation in odd-A nuclei with ground-state spins greater than 1/2, such as one is dealing with here, is complicated by the fact that the second-order effects can involve re-orientation of both the ground and excited states as well as double excitation. In order to calculate all the contributions it is necessary to know both the sign and magnitude of the $B(E2)$ for each level as well as those connecting various levels. The Coulomb excitation cross section between the ground state x of a nucleus and some excited state y can be written

$$d\sigma_{xy} = d\sigma_{xy}^{(1)} + \sum_{z} d\sigma_{xzy}^{(1,2)}, \tag{21}$$

where it can be shown that the higher order terms are negligible. The direct term $d\sigma_{xy}^{(1)}$ is proportional to $B_{xy}(E2)$ while the interference terms $d\sigma_{xzy}{}^{(1,2)}$ are proportional to $(B_{xz}(E2)\ B_{zy}(E2))^{1/2}$. For convenience, the levels in Cu^{63} at 0, 0.668, 0.961, 1.327 and a fictitious level at 2.00 Mev with spins and parities of 3/2-, 1/2-, 5/2-, 7/2- and 3/2- (assumed) will be labelled 0, 1, 2, 3, 4, respectively. Using these labels, the only $B(E2)$'s which are known experimentally are $B_{00}(E2)$, $B_{01}(E2)$, $B_{02}(E2)$ and $B_{03}(E2)$. It is therefore necessary to estimate the other $B(E2)$'s which are required. These estimates have been made and the second-order calculations have been carried out for Cu^{63} by HARVEY and VOGT[42]. The ratio of $B_{33}(E2)$ to $B_{03}(E2)$ can be obtained from the BAYMAN-SILVERBERG model[1]. It depends on the coupling strength y (see ref. 1) but deviates appreciably from the strong coupling value only for $y < 0.1$ where the ratio approaches zero. It has therefore been assumed that $B_{33}(E2)/B_{03}(E2)$ has the strong coupling limit value of 0.11[42]. The other $B(E2)$'s involve transitions within or between the levels 1, 2 and 3 and are equal to $B_{33}(E2)$ multiplied by the ratio of two vector coupling coefficients of the symplectic group[1]. These coefficients are not

TABLE X

Second-order coulomb excitation cross sections for Cu^{63}.

First-order process	Second-order process	$d\sigma^{(1,2)}/d\sigma^{(1)}$
0–1	0–0–1	+0.045
	0–2–1	0.045
	0–4–1	0.045
0–2	0–0–2	+0.045
	0–2–2	0.018
	0–1–2	0.003
	0–3–2	0.041
	0–4–2	0.024
0–3	0–0–3	−0.022
	0–3–3	+0.039
	0–2–3	0.012
	0–4–3	0.010

For notation see appendix II. In column 3 unless the sign is given it is not known.

available and will be assumed to be of the order of unity, giving $B_{12}(E2) = B_{21}(E2) = B_{22}(E2) = B_{23}(E2) = B_{32}(E2) = B_{33}(E2) = 0.11 \times B_{03}(E2)$. The $B(E2)$'s connecting level 4 to levels 0, 1, 2, and 3 have neither been calculated nor measured. They depend on the coupling parameter y in a different way than does $B_{33}(E2)$, and it has arbitrarily been assumed that $B_{04}(E2) = \frac{1}{2}(B_{01}(E2) + B_{02}(E2))$ and $B_{41}(E2) = B_{42}(E2) = B_{43}(E2) = B_{33}(E2)$. With this somewhat arbitrary selection of $B(E2)$'s the ratios $d\sigma^{(1,2)}/d\sigma^{(1)}$ were calculated and are listed in Table XI. The individual contributions range in value from 0.003 to 0.045 but, in general, the relative phases are unknown. The maximum effect for the 0.668 Mev level can be 13.5 %, for the 0.961 Mev level 13.1 % and for the 1.327 Mev level 4.9 %. These are important contributions to the observed values and could be determined with more certainty if the vector coupling coefficients of the symplectic group were known. They are unlikely, however, to have the maximum values.

To investigate the effect of second-order Coulomb excitation on the angular correlations measured in coincidence with back scattered ions detected in a counter near 180°, the following calculation was made, using Beder's computer program[41]. The reaction assumed was that for 34 Mev O^{16} ions incident on Fe^{56} exciting the level at 0.845 Mev. The particle counter was assumed to be a thin ring with the beam as axis making an angle θ_p

TABLE XI

Second-order Coulomb excitation effects on angular correlations of gamma rays measured in coincidence with particles scattered into a ring counter at θ_p with the beam as axis. The calculations are for 34 Mev O^{16} ions on Fe^{56} (thin target) exciting the 0.845 Mev level. The angular correlation is given by $W(\theta_\gamma) = a_0 + a_2 P_2(\cos\theta\gamma) + a_4 P_4(\cos\theta\gamma)$ and a_l^1 includes only first-order effects and a_l^{1+2} includes first plus second.

θ_p	a_0^{1+2}/a_0^1	$\left(\frac{a_2^{1+2}}{a_0^{1+2}}\right)\Big/\left(\frac{a_2^1}{a_0^1}\right)$	$\left(\frac{a_4^{1+2}}{a_0^{1+2}}\right)\Big/\left(\frac{a_4^1}{a_0^1}\right)$
140	1.162	0.994	0.952
150	1.176	0.996	0.979
160	1.186	0.998	0.992
170	1.192	0.999	0.998

with respect to the target center. The computer calculated the coefficients in the Legendre polynomial expansion of the angular distribution given by equation (19) both in first order (a_0^1, a_2^1 and a_4^1) and in first plus second order (a_0^{1+2}, a_4^{1+2} and a_4^{1+2}); the results for various values of θ_p are given in Table XI. It can be seen that for values of $\theta_p > 150°$ the effect on the angular correlations is negligible, although the cross section (proportional to a_0) is strongly affected. The calculations were also made for 32 and 30 Mev O^{16} ions and the effect on the correlations was even smaller. It is clear that no correction from such effects has to be applied to the angular correlations.

Institute for Theoretical Physics
University of Copenhagen.

References

1. B. F. Bayman and L. Silverberg: Nuclear Physics **16**, 625 (1960).
2. Y. Yoshizawa: Physics Letters **2**, 261 (1962).
3. O. Nathan and S. G. Nilsson: Review article to be published in Alpha-, Beta- and Gamma-Ray Spectroscopy, ed. Kai Siegbahn.
4. M. Bouten and P. van Leuven: Nuclear Physics **32**, 499 (1962).
5. A. Blair and D. Armstrong, private communication.
6. R. D. Lawson and J. L. Uretsky: Phys. Rev. **108**, 1300 (1957).
7. A. de Shalit: Phys. Rev. **122**, 1530 (1961).
8. M. Mazari, W. W. Buechner and R. P. de Figueiredo: Phys. Rev. **108**, 373 (1957).
9. G. M. Temmer and N. P. Heydenburg: Phys. Rev. **104**, 967 (1956).
10. For references to properties of levels in Cu^{63} and Cu^{65} from γ-ray measurements, see Nuclear Data Sheets – National Academy of Sciences – National Research Council, Washington, D.C.
11. K. Alder, A. Bohr, T. Huus, B. Mottelson and A. Winther: Revs. Mod. Phys. **28**, 432 (1956).
12. Obtained from R. M. Latimer, Lawrence Radiation Laboratory, University of California, Berkeley, California.
13. Obtained from Oak Ridge Technical Entreprises Corporation, Oak Ridge, Tennessee.
14. Obtained from Hewlett-Packard, Palo Alto, California.
15. Obtained from Oak Ridge National Laboratories, Oak Ridge, Tennessee.
16. We are indebted to Mr. Jørn Borggreen for preparing these targets.
17. A. E. Litherland and A. J. Ferguson: Can. Journal of Phys. **39**, 788 (1961).
18. A. R. Ruthledge CRP-851: Atomic Energy of Canada Limited, Chalk River, Ontario, Canada, July, 1959.
19. D. Eccleshall, B. M. Hinds and M. J. L. Yates: Nuclear Physics **32**, 190 (1962).
20. R. M. Diamond, B. Elbek and F. S. Stephens: Nuclear Physics **43**, 560 (1963).
21. These fits were carried out on the Datatron Computor, Atomic Energy of Canada Limited, Chalk River, Ontario, Canada.
22. R. L. Heath IDO-16408 Phillips Petroleum Co., Atomic Energy Division, Idaho Falls, Idaho, U.S.A.
23. C. Broude and H. E. Gove: Proceedings of the Second Conference on Reactions Between Complex Nuclei, ed. A. Zucker, F. T. Howard and E. C. Halbert. John Wiley and Sons Inc., New York, 1960.

24. B. M. Adams, D. Eccleshall and M. J. L. Yates: Proceedings of the Second Conference on Reactions Between Complex Nuclei, ed. A. Zucker, F. T. Howard and E. C. Halbert. John Wiley and Sons Inc., New York, 1960.
25. D. G. Alkazov, A. P. Grenberg, K. I. Yerokhina and I. Kh. Lemberg: Izvest. Akad. Nauk SSSR Ser. Fiz. **23**, 233 (1959).
26. K. I. Yerokhina and I. Kh. Lemberg: Izvest. Akad. Nauk SSSR Ser. Fiz. **26**, 205 (1962).
27. J. B. Cumming, A. Schwarzochild, A. W. Sunyar and N. T. Porile: Phys. Rev. **120**, 2128 (1960).
28. T. Rothem, E. R. Metzger and C. P. Swann: Bull. Am. Phys. Soc. Ser. 2, **5**, 266 (1960).
29. E. C. Booth: Nuclear Physics **19**, 426 (1960) and E. C. Booth and K. A. Wright, Nuclear Physics **35**, 472 (1962).
30. K. Ilakovac: Proc. Phys. Soc. (London) **67** A, 601 (1954).
31. D. H. Wilkinson: Nuclear Spectroscopy Part B, ed. F. Ajzenberg–Selove, Academic Press, New York, 1960.
32. D. S. Andreyev, A. P. Grenberg, K. I. Yerokhina and I. Kh. Lemberg: Nuclear Physics **19**, 400 (1960).
33. H. E. Gove Physics Letters **4**, 249 (1963).
34. M. Harvey: Nuclear Physics **48**, 578 (1963).
35. Barloutaud, Chaminade, Faraggi, Garetts and Harvey (private communication).
36. The authors are indebted to J. B. French for suggesting this procedure.
37. J. B. French (private communication).
38. W. T. Sharp, J. M. Kennedy, B. J. Sears, and M. G. Hoyle: "Tables of Coefficients for Angular Distribution Analysis" AECL no. 97, Chalk River, Ontario, Canada, August 1954.
39. E. U. Condon and G. H. Shortley: Theory of Atomic Spectra, Cambridge University Press, New York, 1935.
40. We are indebted to Y. Yoshizawa for providing us with this equation.
41. D. Beder: Physics Letters **3**, 206 (1963).
42. M. Harvey and E. Vogt (private communication).

Indleveret til Selskabet den 16. april 1964.
Færdig fra trykkeriet den 17. november 1964.